USAAEFA PROJECT NO. 82-12

12

AD-A141 252

EVALUATION OF UH-1H HOVER PERFORMANCE DEGRADATION CAUSED BY ROTOR ICING

WILLIAM Y. ABBOTT
PROJECT OFFICER/ENGINEER

DAUMANTS BELTE
PROJECT ENGINEER

ROBERT A. WILLIAMS
CW4, AV
PROJECT PILOT

FREDERICK W. STELLAR
CPT, AR
PROJECT PILOT

FINAL REPORT

AUGUST 1983

USAAEFA

UNITED STATES ARMY AVIATION ENGINEERING FLIGHT ACTIVITY
EDWARDS AIR FORCE BASE, CALIFORNIA 93523

DISCLAIMER NOTICE

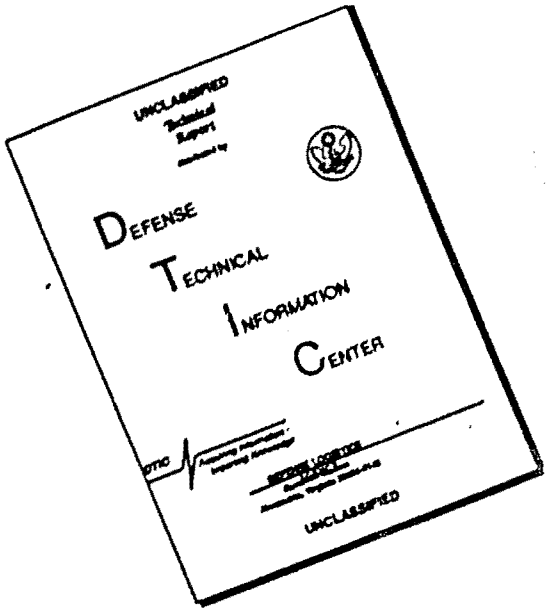

THIS DOCUMENT IS BEST QUALITY AVAILABLE. THE COPY FURNISHED TO DTIC CONTAINED A SIGNIFICANT NUMBER OF PAGES WHICH DO NOT REPRODUCE LEGIBLY.

DEPARTMENT OF THE ARMY
HEADQUARTERS, US ARMY AVIATION SYSTEMS COMMAND
4300 GOODFELLOW BOULEVARD, ST. LOUIS, MO 63120

REPLY TO
ATTENTION OF

DRSAV-E

SUBJECT: Directorate for Engineering Position on the Final Report of USAAEFA Project No. 82-12, Evaluation of UH-1H Hover Performance Degradation Caused by Rotor Icing

SEE DISTRIBUTION

1. The purpose of this letter is to establish the Directorate for Engineering position of the subject report. The objective of the evaluation was to obtain comparative hover performance and blade surface topography data for a clean and an iced rotor system on the UH-1H. The evaluation was conducted in support of AVSCOM and NASA-Lewis requirements to develop a capability to predict analytically the performance penalties associated with helicopter operations in icing conditions. The basic methodology selected to obtain the performance data had not been attempted before and it was recognized early on that the evaluation results could be unreliable for use in verifying NASA-Lewis predictive performance codes. The flight test methods used to obtain performance data are well documented in the report.

2. This Directorate agrees with the report conclusions. However, testing in which ice was accreted on the helicopter rotor blades was done using the Canadian National Research Council (NRC) Icing Spray Rig in Ottawa, Canada. While all testing was done in a hover the data compiled is to be used to predict level flight performance. Consequently, correlation of performance to level flight data is questionable for use for predictive codes. Additionally, hover perfomance testing was conducted in winds up to eight knots as the rotor system was iced behind the Icing Spray Rig. Winds this high make the performance data questionable even though USAAEFA obtained additional clean rotor performance data in similiar winds for comparison.

3. The evaluation documented in the report indicates that the data obtained is questionable for use to validate the NASA-Lewis predictive codes. However indications are that by modifying the methodology based on this evaluation it could result in obtaining usable data for substantiating predictive codes. AVSCOM and NASA-Lewis agreed to conduct another evaluation per USAAEFA Project No. 83-23, "Evaluation of UH-1H Level Flight Performance Degradation Caused by Rotor Icing." This evaluation is being conducted during the 1983/1984 icing season at Duluth, MN. The intent is to attempt to obtain more realistic performance data in level flight using the Helicopter Icing Spray System (HISS).

DRSAV-E

SUBJECT: Directorate for Engineering Position on the Final Report of USAAEFA Project No. 82-12, Evaluation of UH-1H Hover Performance Degradation Caused by Rotor Icing

4. It is important to note that the subject report documents flights testing c a research nature to develop flight test methodology as well as obtaining impor tant performance data related to ice accretion characteristics. The follow-on testing per USAAEFA Project No. 83-23 will expand on the preceding and also program in devising new methodology related to icing testing as well as support NASA-Lewis test requirements.

FOR THE COMMANDER:

RONALD E. GORMONT
Acting Director of Engineering

UNCLASSIFIED

SECURITY CLASSIFICATION OF THIS PAGE (When Data Entered)

REPORT DOCUMENTATION PAGE		READ INSTRUCTIONS BEFORE COMPLETING FORM
1. REPORT NUMBER USAAEFA PROJECT NO. 82-12	2. GOVT ACCESSION NO. AD-A1247	3. RECIPIENT'S CATALOG NUMBER 153
4. TITLE (and Subtitle) EVALUATION OF UH-1H HOVER PERFORMANCE DEGRADATION CAUSED BY ROTOR ICING		5. TYPE OF REPORT & PERIOD COVERED 28 JAN - 4 MAR 1983 FINAL 6. PERFORMING ORG. REPORT NUMBER
7. AUTHOR(s) WILLIAM Y. ABBOTT ROBERT A. WILLIAMS DAUMANTS BELTE FREDERICK W. STELLAR		8. CONTRACT OR GRANT NUMBER(s)
9. PERFORMING ORGANIZATION NAME AND ADDRESS US ARMY AVN ENGINEERING FLIGHT ACTIVITY EDWARDS AIR FORCE BASE, CA 93523		10. PROGRAM ELEMENT, PROJECT, TASK AREA & WORK UNIT NUMBERS EK3PW313EKEC
11. CONTROLLING OFFICE NAME AND ADDRESS US ARMY AVN RESEARCH & DEVELOPMENT COMMAND 4300 GOODFELLOW BOULEVARD ST. LOUIS, MO 63120		12. REPORT DATE AUGUST 1983 13. NUMBER OF PAGES 71
14. MONITORING AGENCY NAME & ADDRESS(if different from Controlling Office)		15. SECURITY CLASS. (of this report) UNCLASSIFIED 15a. DECLASSIFICATION/DOWNGRADING SCHEDULE

16. DISTRIBUTION STATEMENT (of this Report)

Approved for public release; distribution unlimited.

17. DISTRIBUTION STATEMENT (of the abstract entered in Block 20, if different from Report)

18. SUPPLEMENTARY NOTES

19. KEY WORDS (Continue on reverse side if necessary and identify by block number)

Hover Icing
UH-1H Helicopter
Ice Shapes
Low-speed Performance

20. ABSTRACT (Continue on reverse side if necessary and identify by block number)

The US Army Aviation Engineering Flight Activity conducted hover icing tests with a UH-1H helicopter, for NASA Lewis Research Center. The rotor blade ice shapes obtained in the Canadian National Research Council Icing Spray Rig were documented using steroscopic photography, silicone molds, and cross-section tracings. Power required data were also obtained in an attempt to define the rotor performance degradation caused by icing. A summary of the test effort and ice shape documentation is presented in this report. Additional low-speed performance tests were performed and the results presented.

DD FORM 1 JAN 73 1473 EDITION OF 1 NOV 65 IS OBSOLETE

UNCLASSIFIED

SECURITY CLASSIFICATION OF THIS PAGE (When Data Entered)

TABLE OF CONTENTS

INTRODUCTION

BACKGROUND

1. The Applied Technology Laboratory (ATL), Research and Technology Laboratories, US Army Aviation Research and Development Command (AVRADCOM), and the NASA Lewis Research Center (NASA Lewis) are jointly undertaking a program to predict the hover performance penalties associated with helicopter operations in icing conditions. The phases of the program include flight test, wind tunnel tests, and computer modeling. In October, 1982, AVRADCOM, at the request of NASA Lewis, directed the US Army Aviation Engineering Flight Activity (USAAEFA) to conduct the flight test portion of the program (ref 1, app A), and a test plan was prepared (ref 2). The Aeronautical and Astronautical Research Laboratory of Ohio State University (OSU) was contracted to document the ice shapes obtained during flight tests, and conduct subsequent wind tunnel experiments on the shapes. Bell Helicopter Textron (BHT), Texas Agricultural and Mechanical University (Texas A&M), and NASA Ames Research Center (NASA Ames) were contracted to analyze the combined flight and wind tunnel data and develop the mathematical algorithms required to predict hover performance degradation caused by rotor icing.

2. The flight test portion of the program consisted of gathering hover performance data with both clean and iced rotor blades, and documenting the topography of the ice accretion. The icing tests were conducted using a UH-1H helicopter at the Canadian National Research Council (NRC) Icing Spray Rig in Ottawa, Canada.

TEST OBJECTIVE

3. The objective of the flight tests was to gather comparative hover performance and blade surface topography data for the UH-1H helicopter with both clean and iced rotor blades. Because the NRC Icing Spray Rig requires a minimum wind velocity of 6 knots, true hover data in still air would not be possible. Therefore, a secondary objective was to evaluate the low-speed performance characteristics of the aircraft.

DESCRIPTION

4. The UH-1H is a thirteen-place single engine helicopter using a single two-bladed teetering main rotor and a two-bladed tail rotor. The maximum gross weight is 9500 pounds. Power is provided by a Lycoming T53-L13B free turbine engine rated at 1400 shaft horsepower (SHP) at sea level standard day conditions. The main rotor transmission is limited to 1100 SHP for continuous operation. The test aircraft, US Army serial number 69-15532,

(photo 1) is a standard production UH-1H equipped with test instrumentation, a rotor brake, and a heated windshield. A more complete description of the aircraft is contained in the operator's manual (ref 3).

5. The NRC spray rig (photos 2 and 3) consists of 156 steam atomized water nozzles mounted on a steel framework 50 feet high. The nozzle array may be rotated $\pm$180 degrees to take advantage of winds from any direction. Proper formation of ice cloud requires steady winds from 6 to 25 knots. A more detailed description of the icing spray rig is contained in reference 4 and appendix B.

TEST SCOPE

6. Icing flight tests were conducted at the NRC Icing Spray Rig at Ottawa (elevation 374 feet) between 28 January and 4 March 1983. Eleven flights were made totalling 8.1 hours. Eight low-speed and hover flights, totalling 8.4 hours were made at Edwards Air Force Base, California (elevation 2303 feet) between 22 April and 6 June 1983. Test conditions are discussed in the Results and Discussion section of this report. An additional 54.6 hours were flown during ferry and checkout flights.

TEST METHODOLOGY

7. Test data were obtained from sensitive instrumentation displayed to the pilots and recorded on magnetic tape. A detailed listing of the test instrumentation is contained in appendix C. Test techniques are described in the Results and Discussion section, and analysis procedures are described in appendix D.

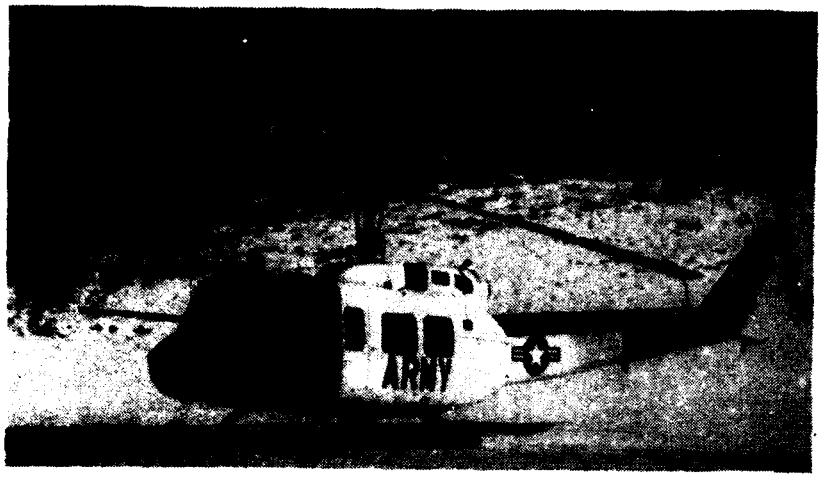

Photo 1. UH-1H Helicopter S/N 69-15532

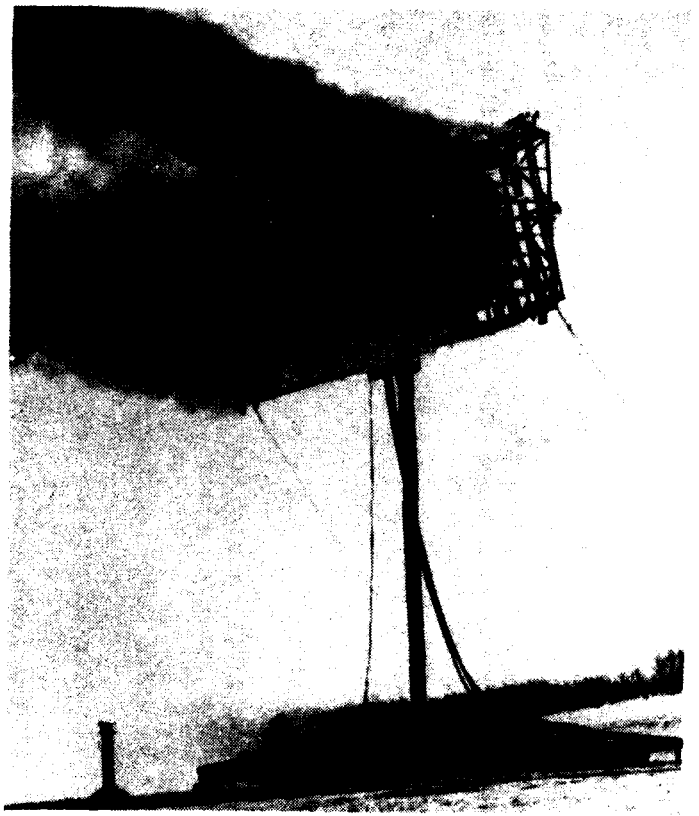

Photo 2. NRC Icing Spray Rig

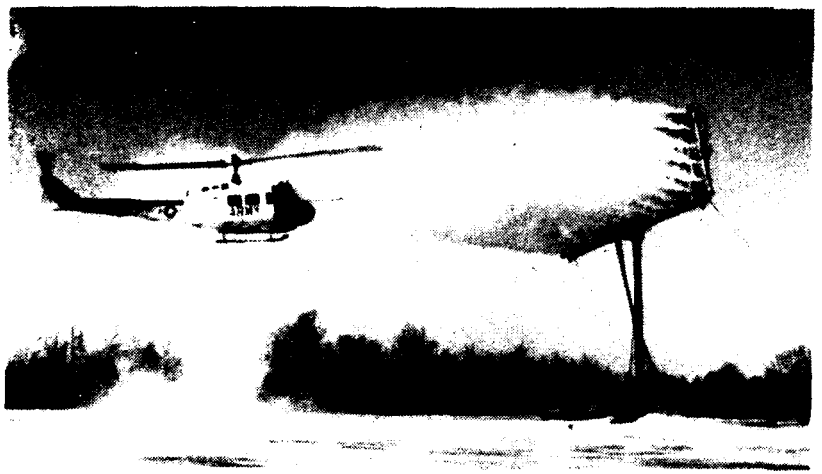

Photo 3. UH-1H in Spray Rig

RESULTS AND DISCUSSION

GENERAL

8. The intent of this program was to provide data for correlation of hover performance degradation with specific ice contours. The first technique attempted was to fly several tethered hover points, release the tether, enter the ice cloud and gather ice, exit the cloud, attach the tether, and repeat the tethered hover points. However, the flexing of the rotor blades during the second series of hover points shed most of the ice accreted in the cloud.

9. The technique finally established was to:

a. Determine baseline profile power required by doing a flat-pitch ground run at several rotor speeds

b. Fly a baseline out-of-ground effect (OGE) free hover point

c. Enter the cloud, accrete ice, and exit the cloud

d. Fly another free hover point to determine hover performance degradation

e. Repeat the flat-pitch ground run to determine the increase in profile power caused by icing

f. Document the ice shapes

This technique allowed the ice to remain on the blades without shedding.

10. Ten flights behind the rig were made, with ice being retained on five. Each successful icing flight was assigned a letter by NASA Lewis. Flight conditions are shown in table 1. Spanwise ice formation was noted for all flights, and is presented with temperature in figure 1. Above a temperature of -9.5°C, adequate ice could not be retained.

11. The icing spray rig requires a minimum of 6 knots wind to form a cloud a safe distance from the rig itself. Therefore, it is impossible to obtain true hover data while the rig is in operation. Additional low-speed flights were flown at Edwards Air Force Base to provide data relating hover and low wind speed performance.

Table 1. Icing Rig Test Conditions and Documentation

NASA Test	Wind		Water flow (lb/hr)	LWC[1] (gm/m^3)	Temperature (°C)	Sky Condition	Time in Cloud (min)	Ice		Documentation
	Speed (knots)	Gustiness						Thickness at BS[2] 144 (in.)	Maximum Span (%)	
A	7	Medium	4400	0.4	-12.0	Overcast	4-1/2	0.2	75	Molds Tracings Stereo Photos
B	10	Medium	6200	0.4	-9.5	Overcast	4-1/4	0.3	65	Molds Tracings Stereo Photos
C	6	Medium	4000	0.4	-17.5	Clear	4	not measured	85	Molds Stereo Photos
D	4	Low	2600	0.4	-21.5	Clear	6	0.2	92	Molds Tracings
E	9	Low	6200	0.7	-19.0	Clear	3	0.4	92	Molds Tracings Stereo Photos

NOTES:

[1]LWC = Liquid water content as determined by NRC
[2]B.S. = Blade station

FIGURE 1

SPAN-WISE ICE RETENTION WITH TEMPERATURE

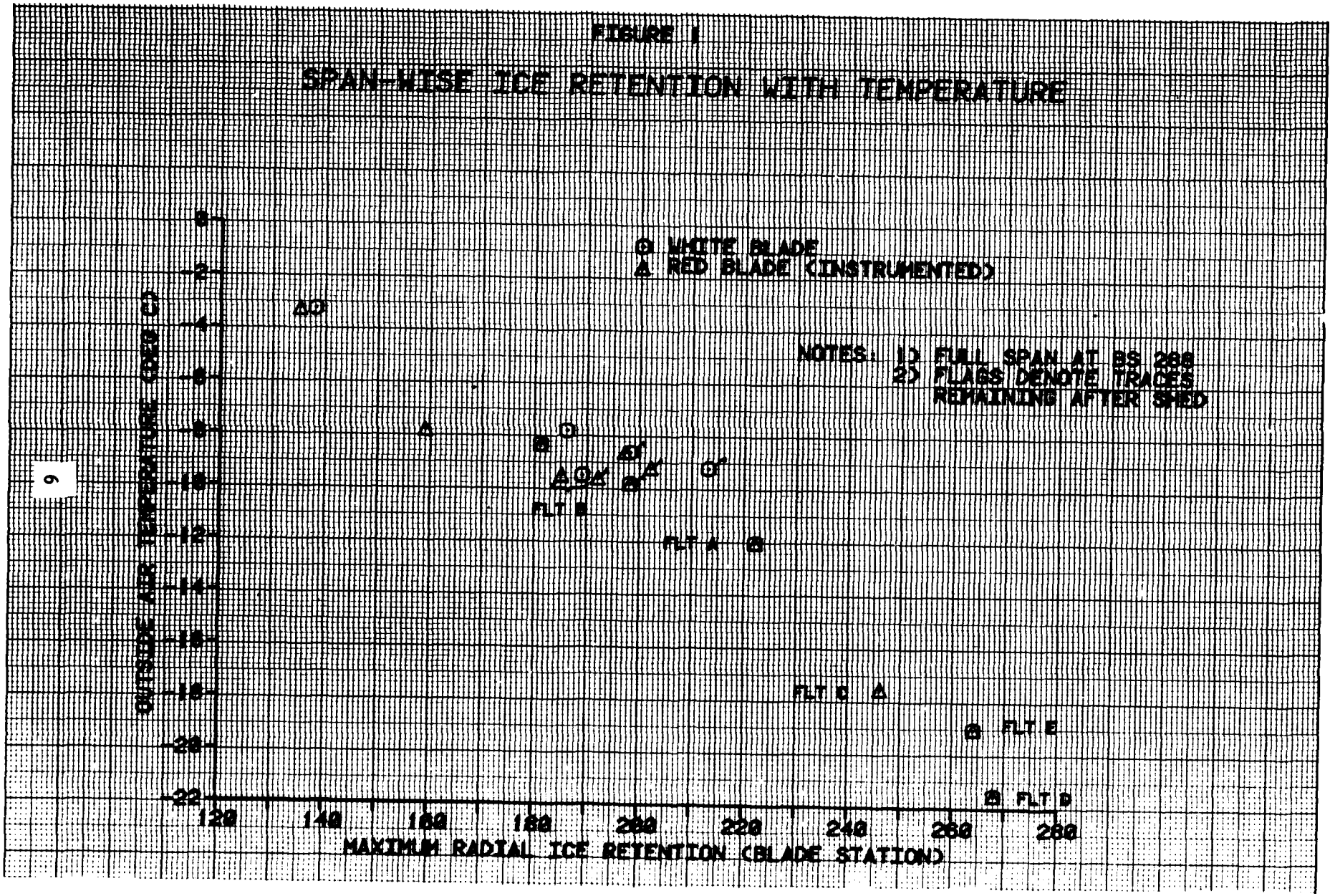

ICE DOCUMENTATION

General

12. OSU had general management responsibility for the documentation of ice shapes. Arvin/Calspan Field Services, Inc., at Arnold AFS, Tennessee had the responsiblity for the research and development of stereoscopic photography techniques and computer interpretation. A local Ottawa firm, Hovey and Associates (1979) Ltd., actually performed all the documentation activities at the ice rig. The three documentation methods used were molding, tracings, and stereoscopic photography.

13. All the documentation efforts took place in a special work platform; a modified airline galley truck borrowed from Air Canada (photos 4 and 5). The truck had inside dimensions of 20 feet long by 7-1/2 feet wide by 7 feet high with a 4-foot wide door. Modifications to the truck included installing three 100 vac duplex outlets, four 750 watt, 220 vac space heaters, and a 1500 watt, 110 vac heater. The rotor blade being documented was positioned perpendicular to the aircraft centerline, and the work platform was backed up so the blade was within the truck. The blade tip was then secured to the platform with a fixture. The door was partially closed vertically from the top and a tarp was attached below the door to seal the truck from the outside conditions. The heaters were used to slowly increase the temperature to a maximum of -5°C.

Steroscopic Photography

14. A stereo-photogrammetic technique developed by Arvin/Calspan Field Services Inc. for the Arnold Engineering Development Center (AEDC) of the Air Force Systems Command was one of the methods used to document the ice formations on the rotor blade. In this technique, wide-angle stereo photographs of the test contour were taken by two cameras oriented on converging axes while the target was illuminated by a projected grid pattern. An additional target screen fixture with marked control points at known coordinates was placed within the field-of-view over the blade. By referring to the projected grid, the control point rig, and markings on the blade itself, a computer assisted analysis of the ice shape photographs could be performed to numerically define the contour both in general shape (profile) and fine scale (roughness). A general background and description of the analysis technique using a Keuffel and Esser model DCS-3/80 Analytical Sterocompiler interfaced with the AEDC computer facility is given in reference 5.

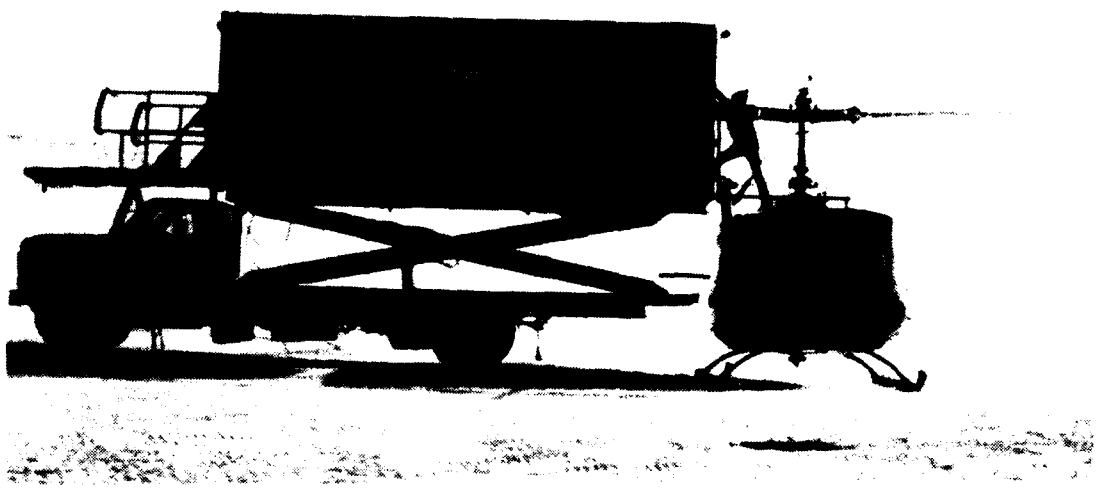

Photo 4. Documentation Work Platform

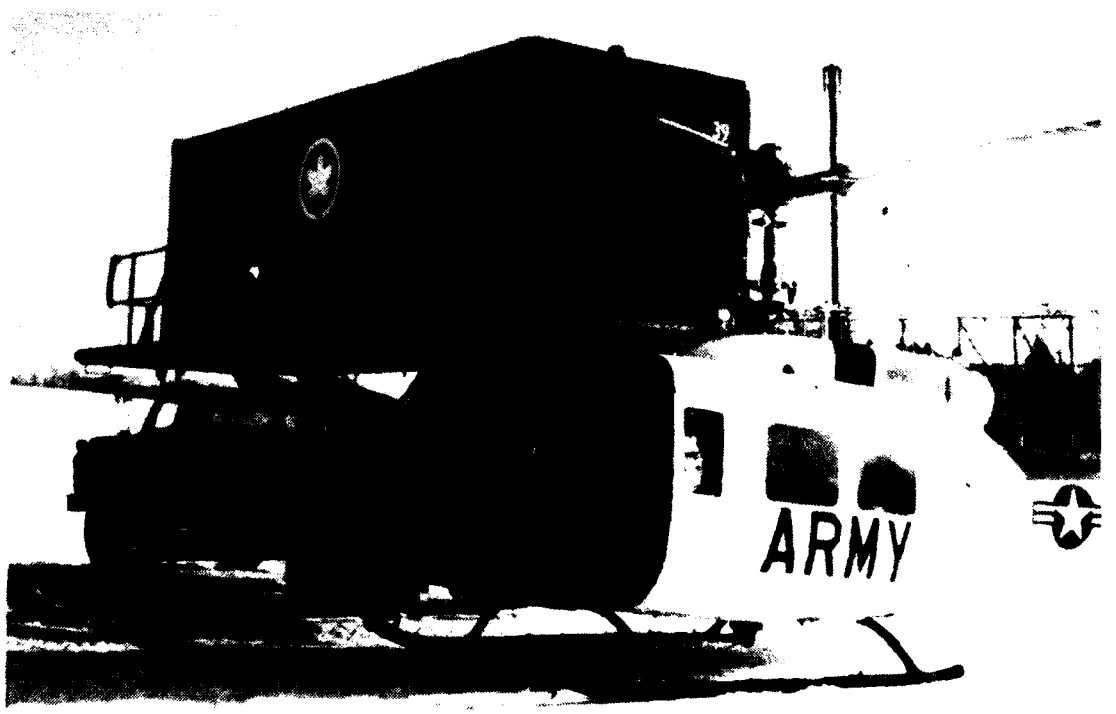

Photo 5. Main Rotor Blade Positioned In Work Platform

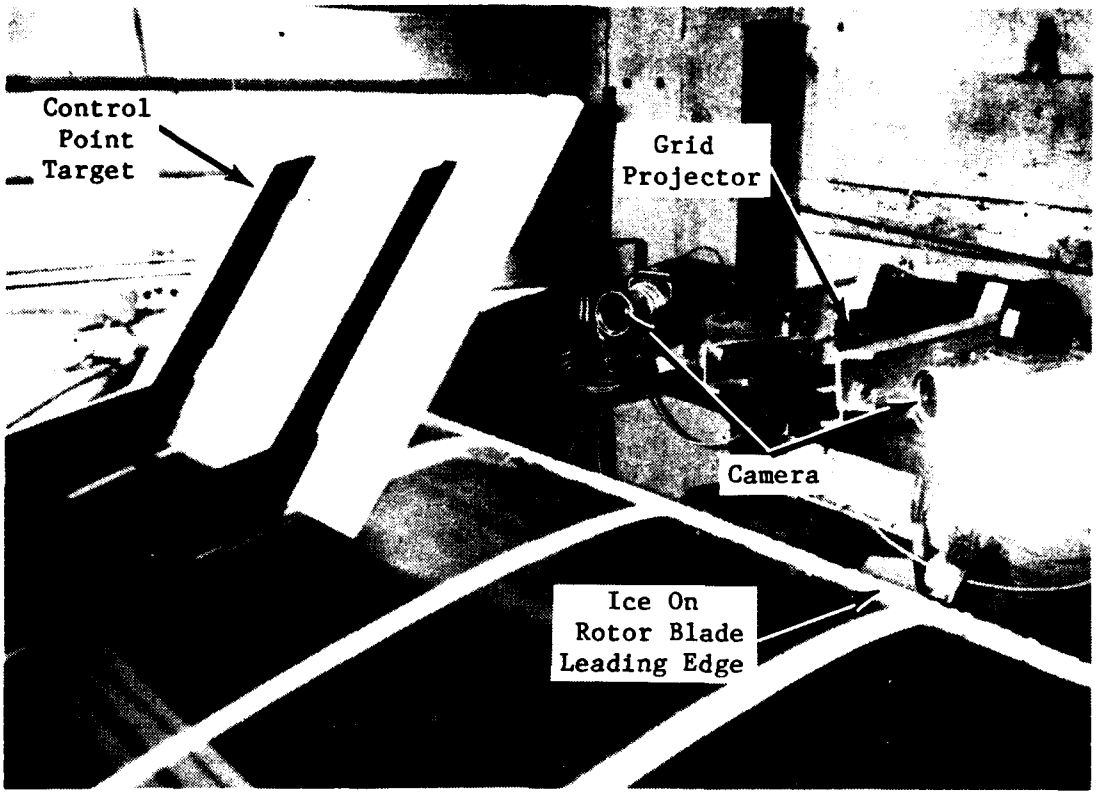

Photo 6. Stereoscopic Cameras Positioned Horizontally Even with the Rotor Blade

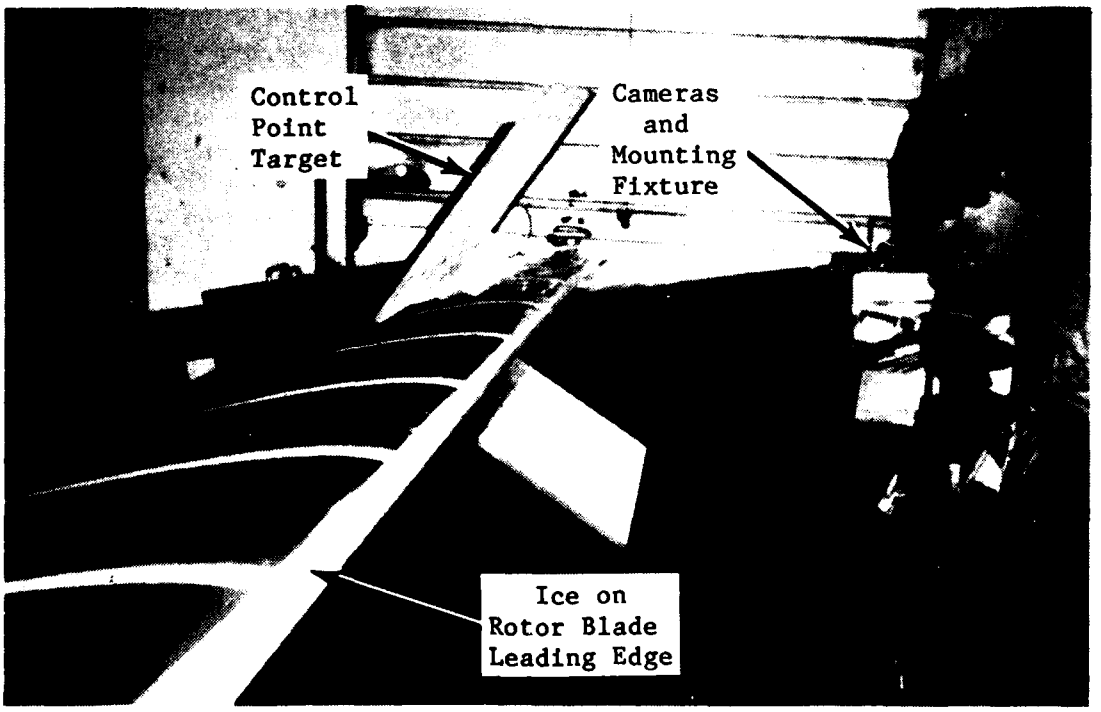

Photo 7. Stereoscopic Cameras Positioned Horizontally Even with the Rotor Blade

15. Each photographic pair was obtained with two 70mm Hasselblad cameras equipped with 50mm lenses attached to a mounting fixture. Black and white Kodak Plus-X Pan (2147) film was used, and the film magazines were modified to ensure that the film was held flat by a vacuum pump during the simultaneous exposures. Overall views of the stero camera test setup are shown in photos 6 and 7, and a 3-view schematic of the general layout used appears in figure 2. The mounting fixture separates the camera lenses by 24 inches horizontally. Once the iced rotor blade was positioned inside the work platform and secured at the tip, the camera rig was situated facing the leading edge of the airfoil at a distance from 18 to 21 inches. The control point rig, consisting of two flat surfaces perpendicular to each other and marked with a pattern of dots, was positioned over the rear of the rotor blade to form the fixed target with known coordinates.

16. A central flash unit located between the cameras projected a grid pattern onto the blade and target, and two synchronized strobe units adjacent to the cameras provided additional illumination to the sides. To provide a better image of the projected grid, the surface of the ice was lightly dusted with a white talc-like powder prior to photography. The rotor blades had 1-inch wide white stripes painted at 1-ft intervals along the span, and a pattern of four black dots were spaced 1 1/2 inches apart on the stripes, starting 3 1/2 inches aft of the leading edge, on both upper and lower blade surfaces.

17. These stereo pairs were taken along the iced span of the blade centered on every second foot-wide segment between the stripe markings. The most inboard segment accessible within the work platform was 5 feet from the hub. A series of three photographs were made at each location as the cameras were adjusted vertically: in the chord plane, and approximately one foot above and below the chord plane.

18. A representative series of photographs from the stereo cameras are shown in photos 8 through 11. These show the ice formations resulting from test flight "E" at blade stations 102 and 222 (8.5 and 18.5 ft from the hub, respectively). Left and right stereo pairs taken from above and beneath the rotor plane are presented. These photographs show the ice accretion, the rotor blade marked with stripes and reference dots, the control point rig with its pattern of target dots, and the projected grid.

19. Analysis by AEDC of the stereo pair photographs was done by reading coordinates with the analytical stereo-compiler directly from the original negatives. The numerical data transmitted to

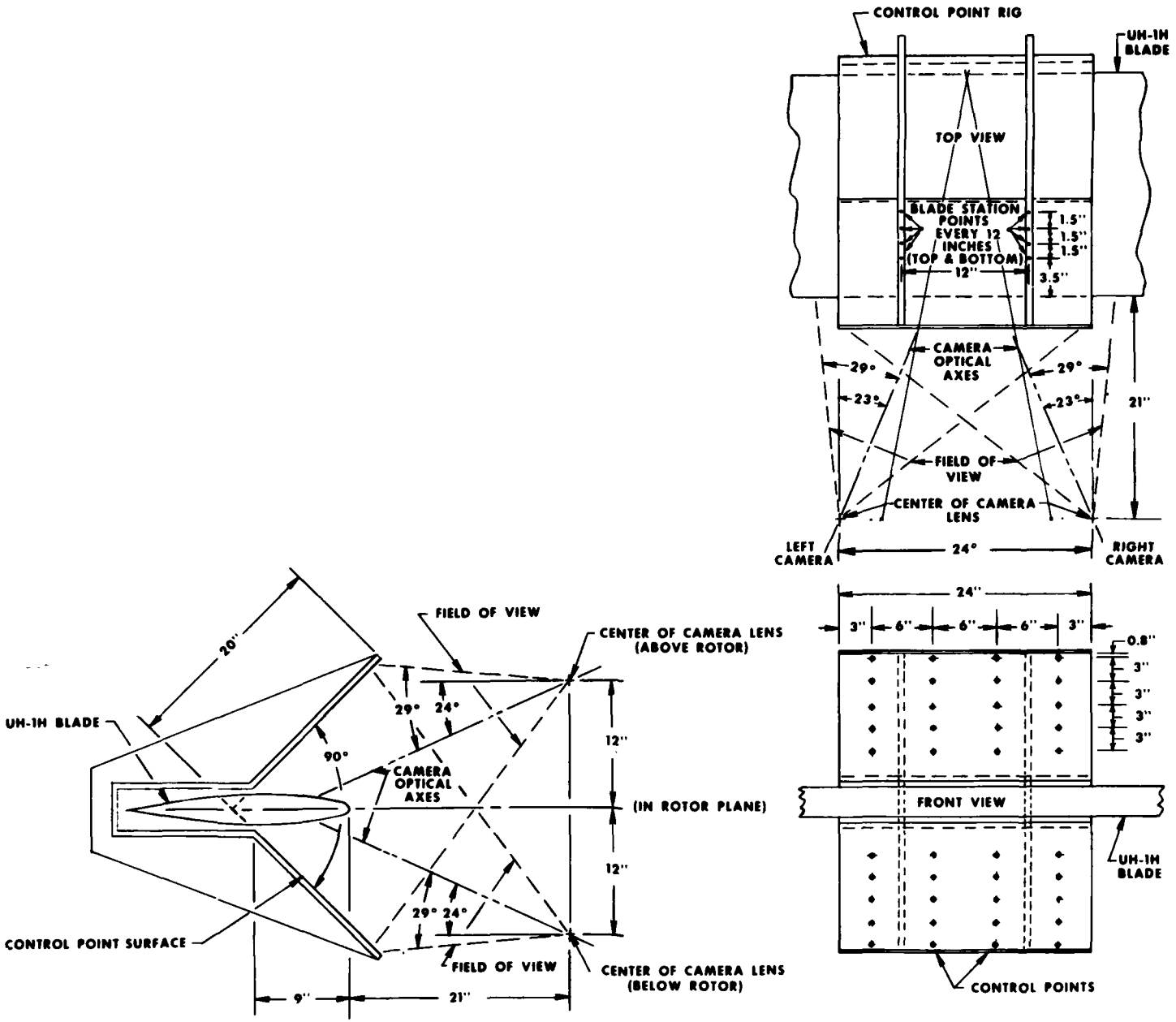

Figure 2. Schematic 3-View of Stereographic Test Set-Up Showing Relative Locations of Rotor Blade, Control Point Rig Target, and Camera Lenses

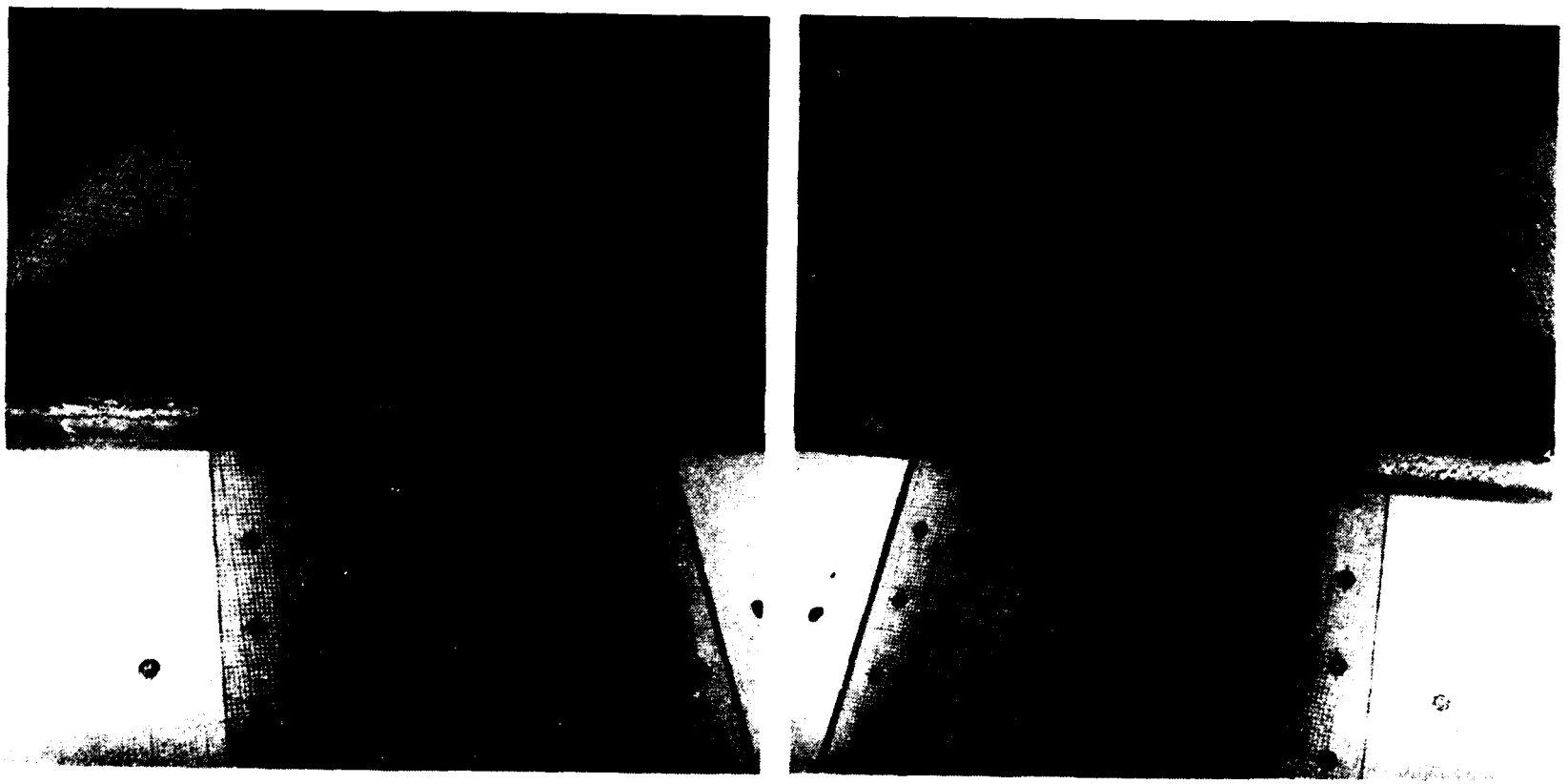

Photo 8. Left and Right Stereo Pair Taken Above the Rotor Plane. Test "E", Blade Station 102 (Centered Between the 8 and 9 ft Stripes from Hub)

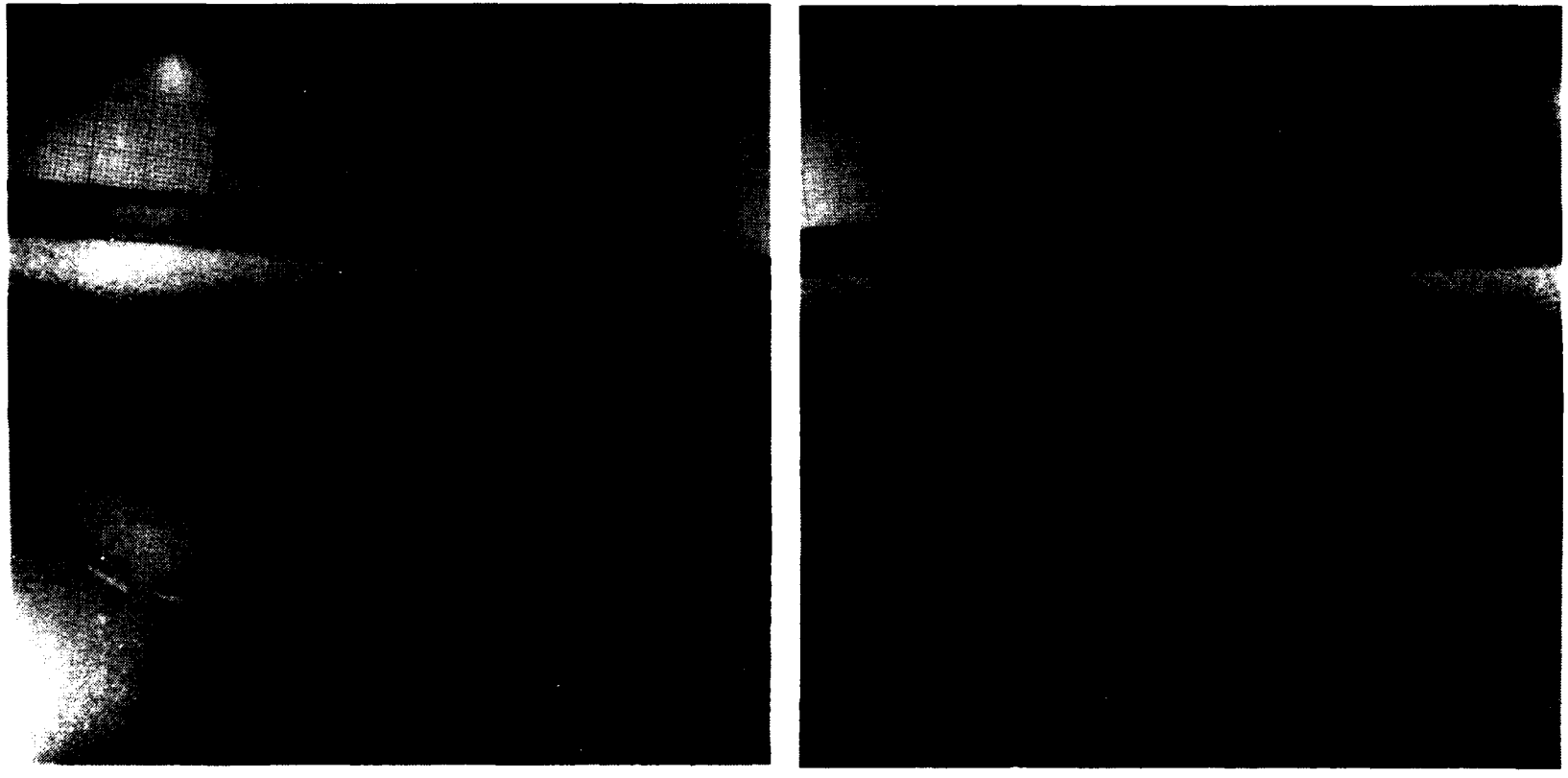

Photo 9. Left and Right Stereo Pair Taken Below the Rotor Plane. Test "E", Blade Station 102 (Centered Between the 8 and 9 ft Stripes from Hub)

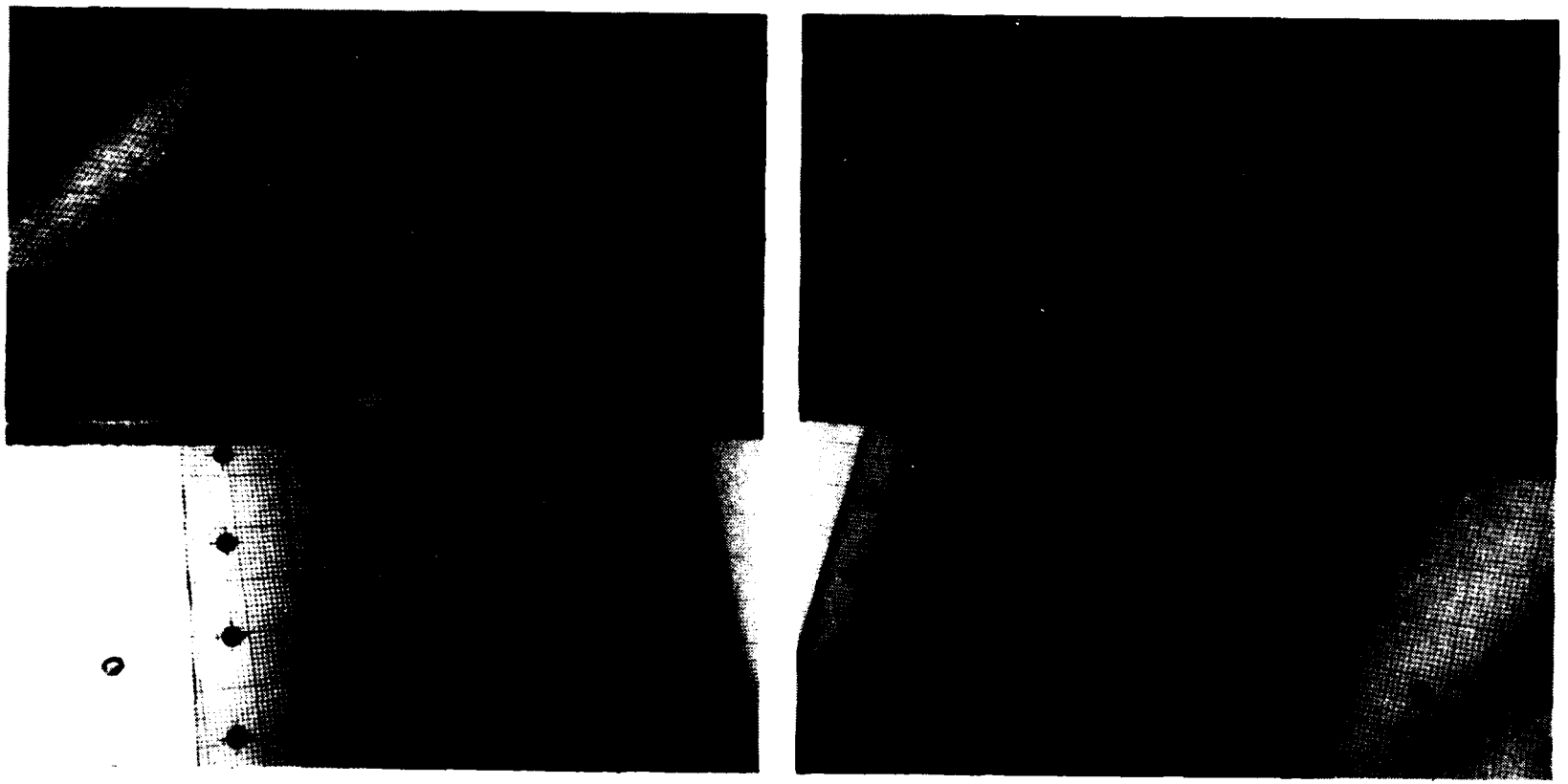

Photo 10. Left and Right Stereo Pair Taken Above the Rotor Plane. Test "E", Blade Station 222 (Centered Between the 18 and 19 Ft Stripes from Hub)

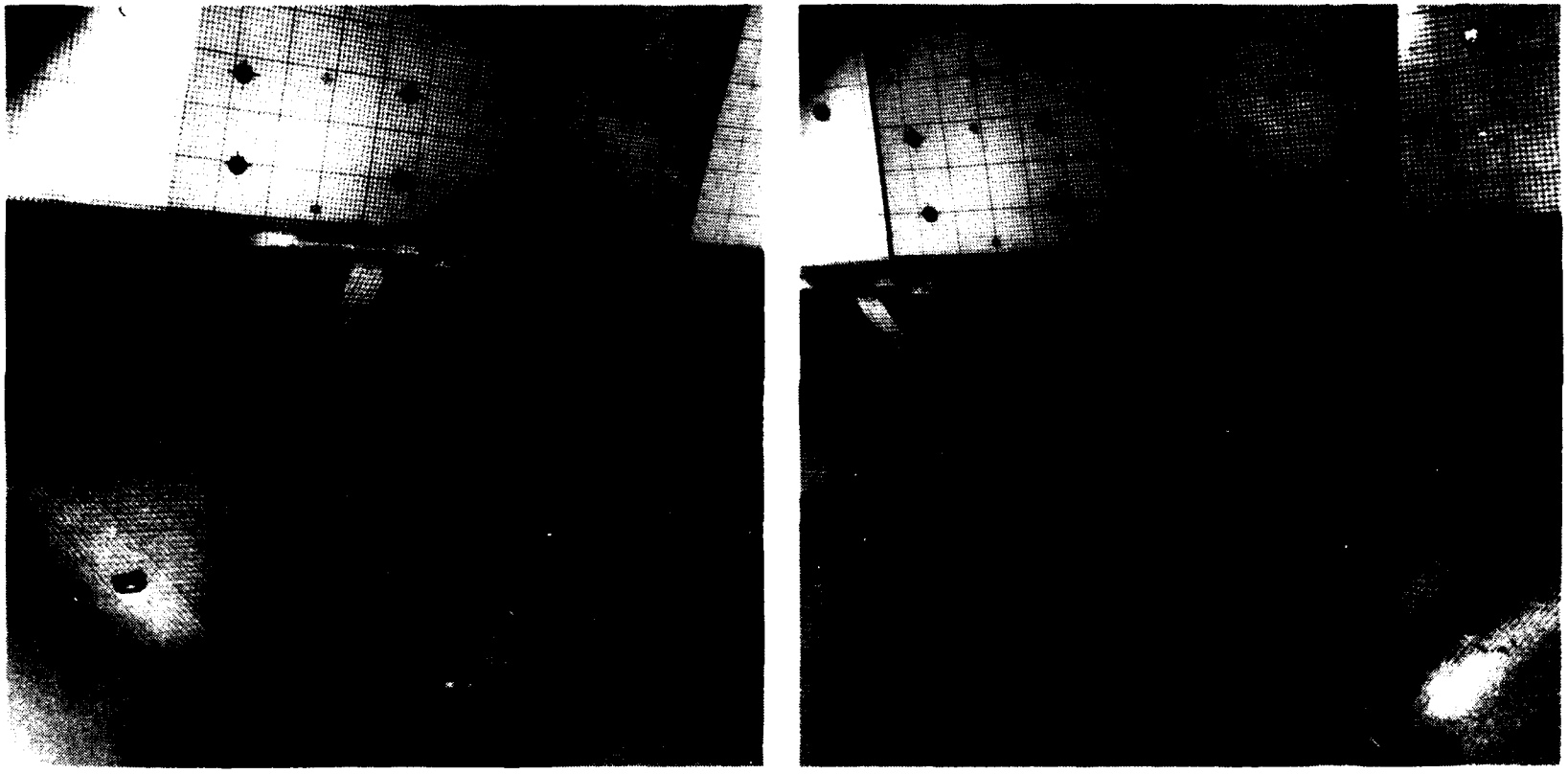

Photo 11. Left and Right Stereo Pair Taken Below the Rotor Plane. Test "E", Blade Station 222 (Centered Between the 18 and 19 Ft Stripes from Hub)

the AEDC computer could then be transformed or rotated within selected coordinate axes as desired for further manipulation. Two types of ice surface analyses were performed by AEDC, giving results such as those shown in figures 3 and 4. Figure 3 presents a set of profile coordinates showing the general shape of the cross-section, figure 4 is a surface roughness analysis showing fine scale spanwise. The horizontal and vertical axes are scaled to represent actual inches, corresponding to reference coordinates used by the AEDC computer. These sample figures represent photogrammetric analysis results of the same stereo pair samples at blade station BS 102 and 122 from test "E" shown previously. The complete stereo compiler results and ice shape analyses of all the stereo photographs taken during this project are presented in reference 6.

Tracings

20. After the stereo photos were taken, a hot wire electric "knife" was used to cut a cross section of the ice shape at two foot intervals along the span of the accreted ice. A template was then inserted against the blade, and a pencil tracing was made of the ice shape. The tracings are shown in figures 5 through 8. The tracings are accurate, and since they can be made quickly and easily, the tracing technique is a valuable documentation method.

Molding

21. One foot wide plywood mold frames (fig. 9) were placed around the blade at two foot intervals along the span of accreted ice (photos 12 and 13). Approximately 1.7 kg of room temperature vulcanizing (RTV) silicone molding compound was poured into each frame, and allowed to cure for 3 hours. Heating pads were placed around the molds after the first hour. The compound was made of 1 part Dow Corning RTV 3110 base, 1/9 part No. 200 thinner, and 1/150 part No. 4 catalyst. Slightly more catalyst was used when temperatures were below -10°C.

22. The base and thinner were pre-measured in 5 kg batches, put into buckets, and stored in an unheated building. Approximately 30 minutes before use, the catalyst was added, and the compound was mixed with an electric drill and paint mixer attachment or paddle. The buckets were then placed in a vacuum chamber for 15 minutes to remove excess air.

23. The compound was made relatively thin to fully contour the ice shapes during molding. The molds set to the point they could be removed from the rotor blade in about 3 hours. They were normally removed from the mold frames the following day.

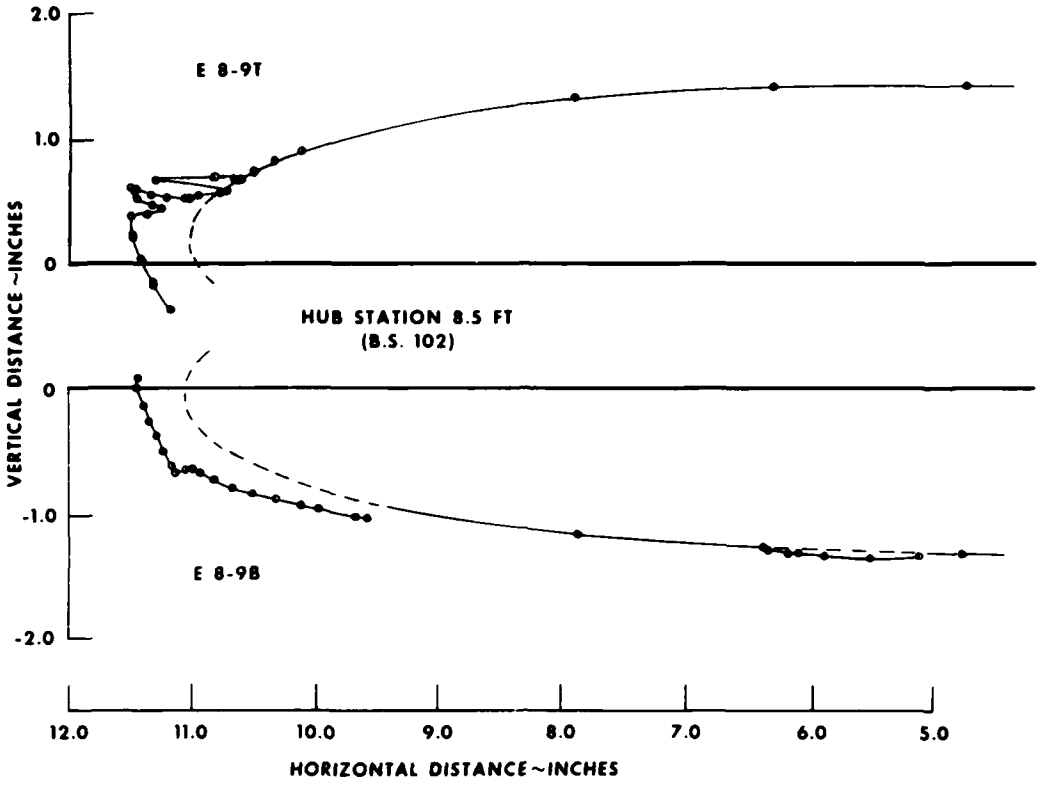

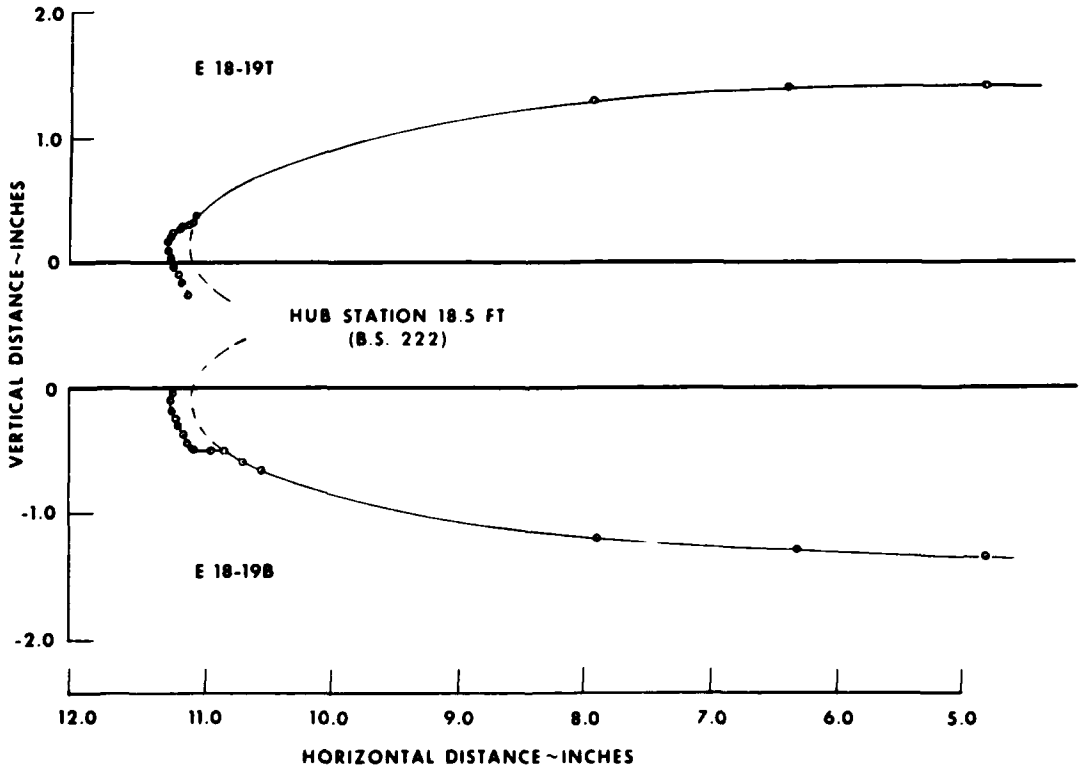

Figure 3. Photogrammetric Analysis Profile Results Showing General Shape of the Ice Accretion. Test "E", Blade Stations 102 and 222

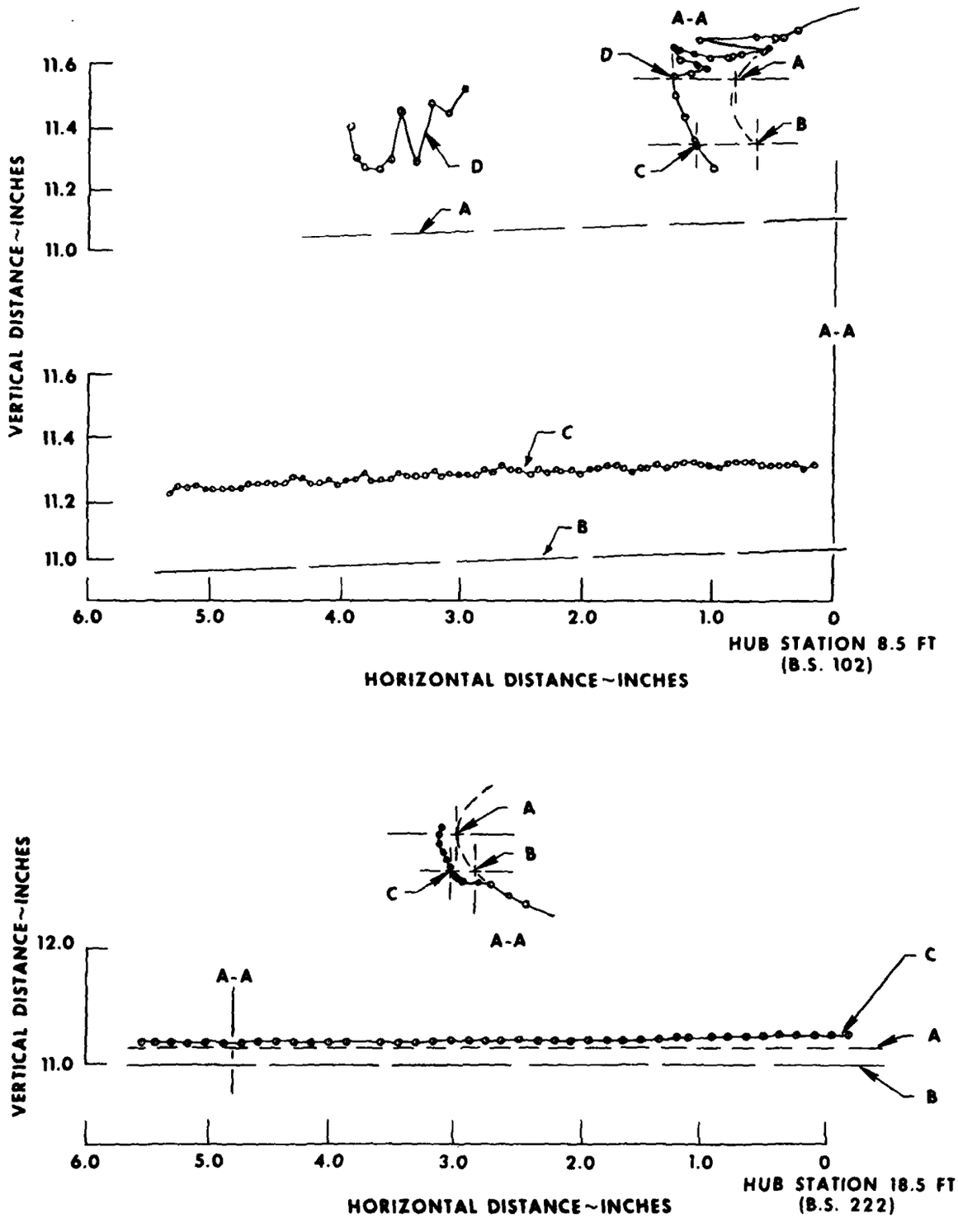

Figure 4. Photogrammetric Analysis Surface Roughness Results Showing Spanwise Ice Accretion in Fine Scale. Test "E", Blade Stations 102 and 222

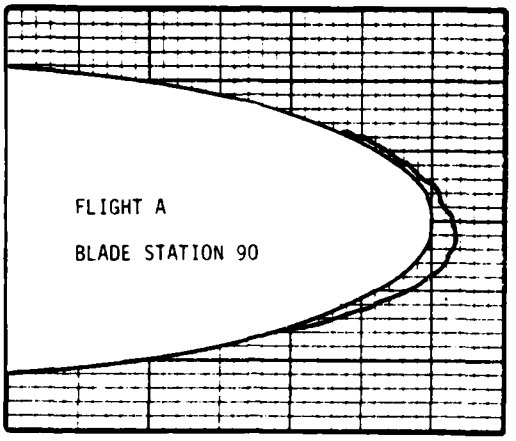

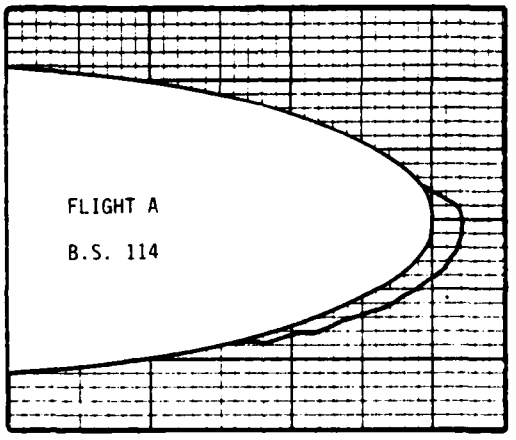

NOTE: MINOR DIVISIONS EQUAL 0.1 INCH

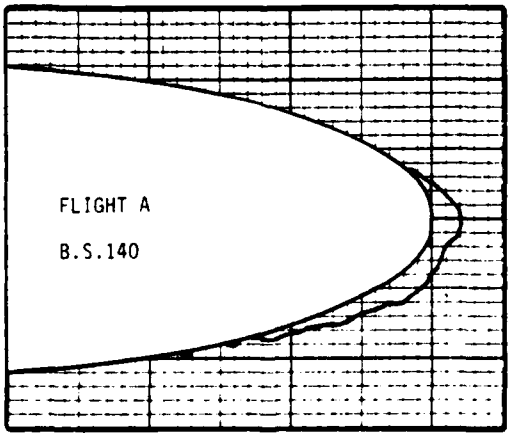

Figure 5. Flight A Ice Shapes From Tracings

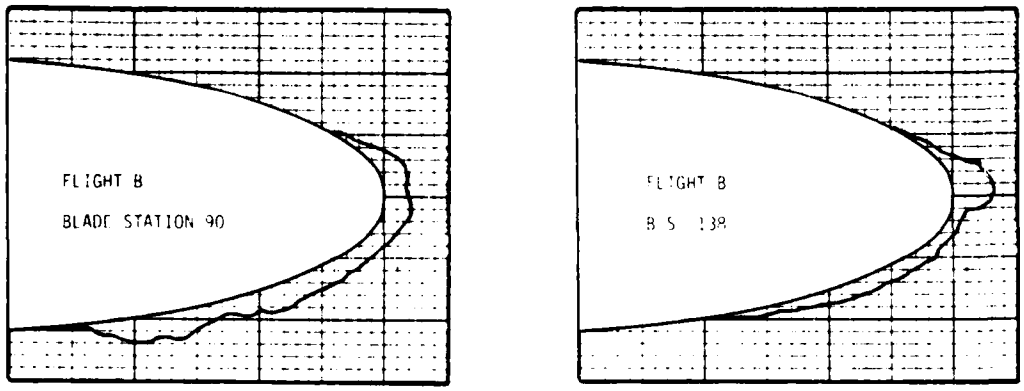

NOTE: MINOR DIVISIONS EQUAL 0.1 INCH

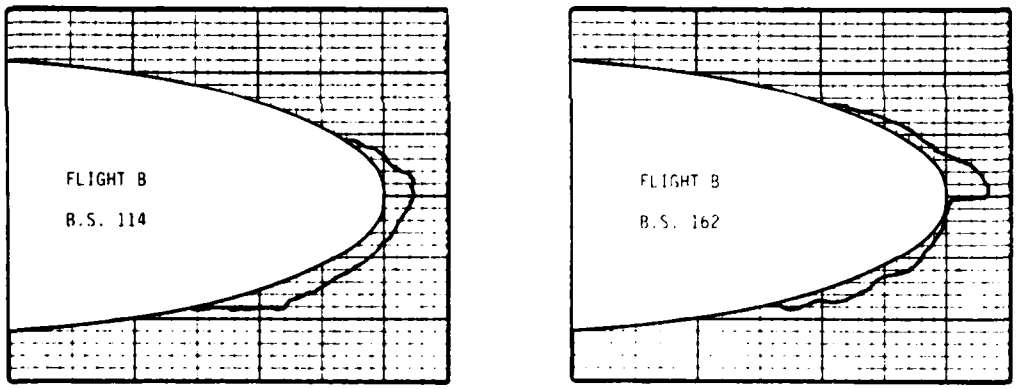

Figure 6. Flight B Ice Shapes From Tracings

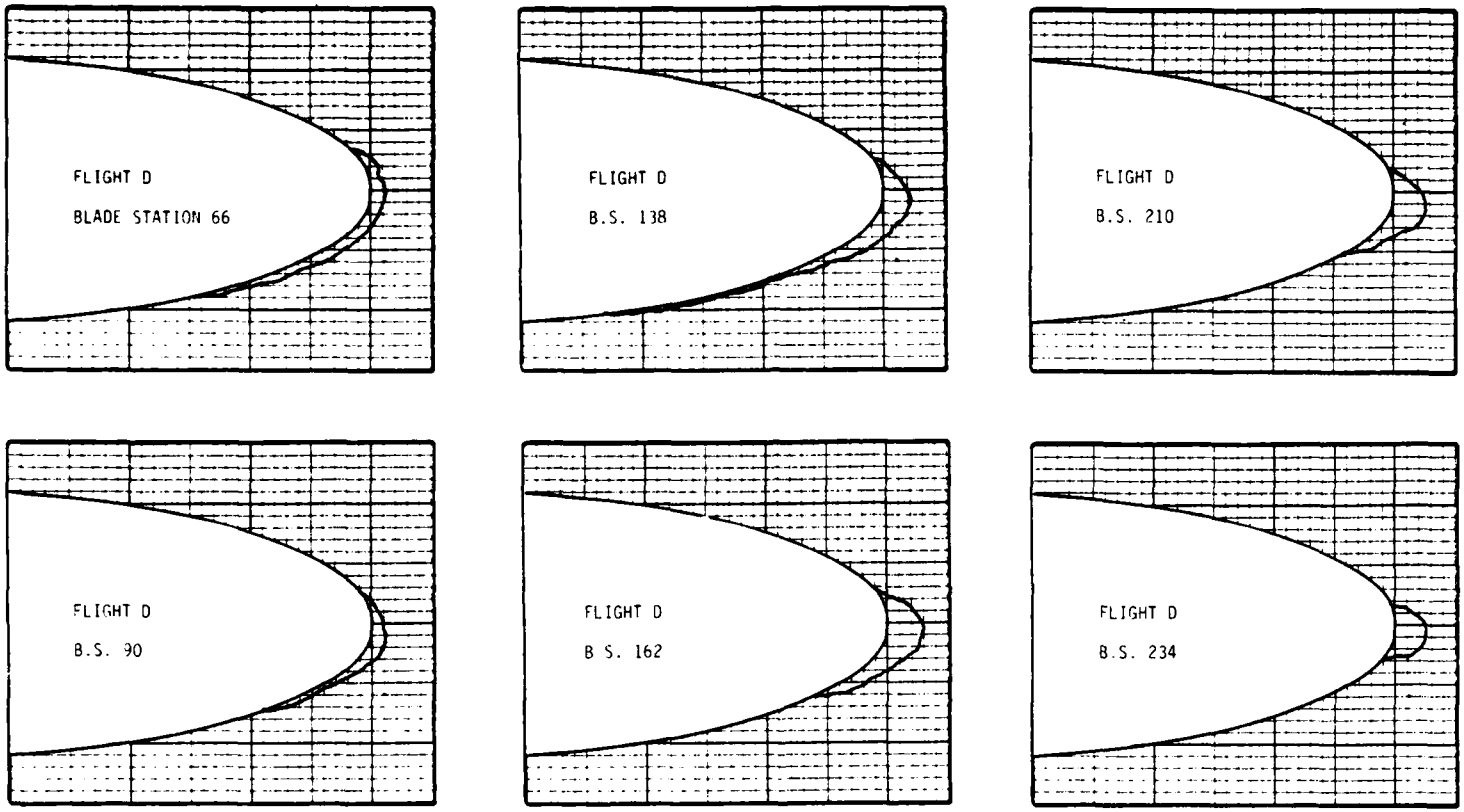

Figure 7. Flight D Ice Shapes From Tracings

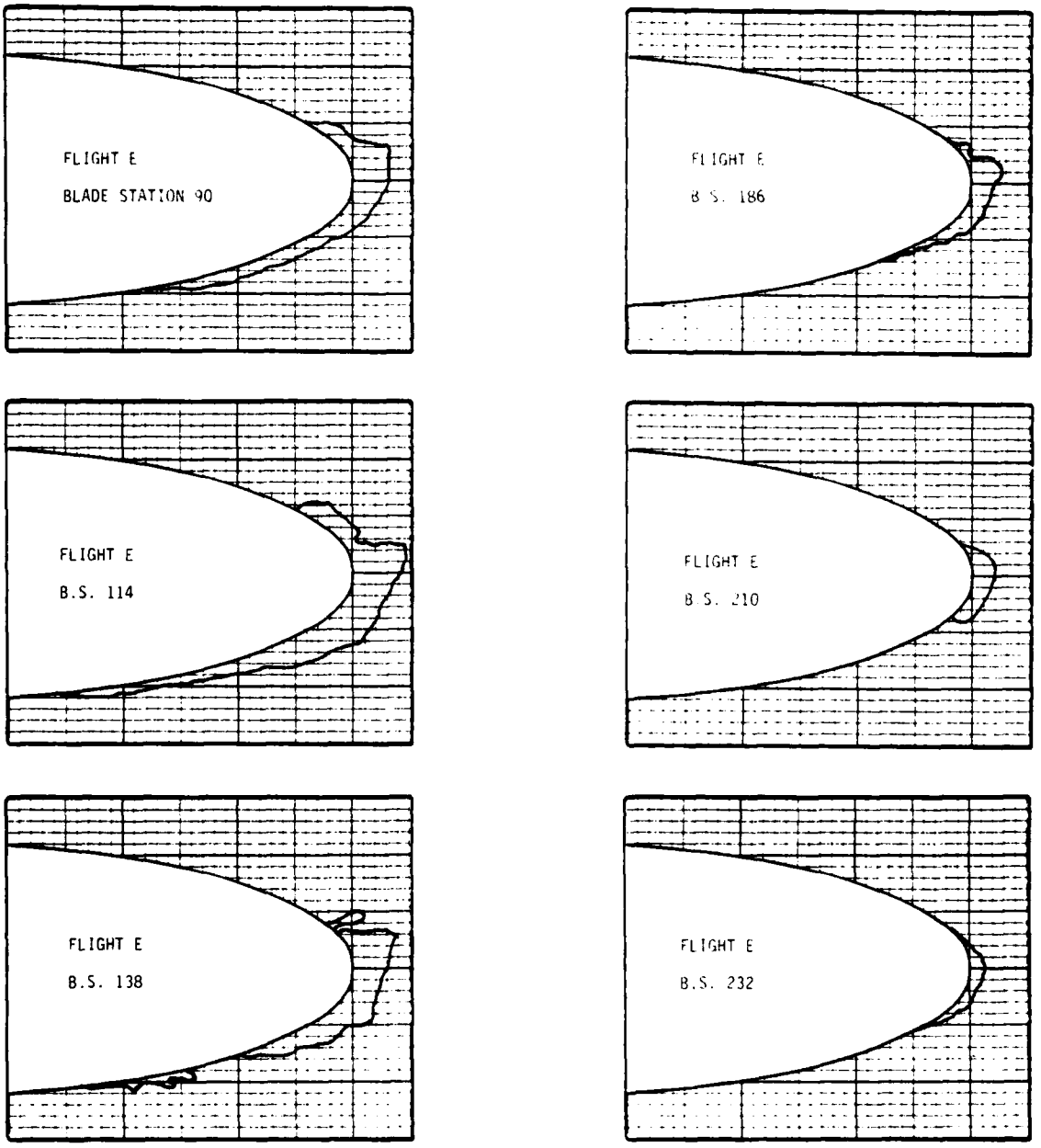

NOTE: MINOR DIVISIONS EQUAL 0.1 INCH

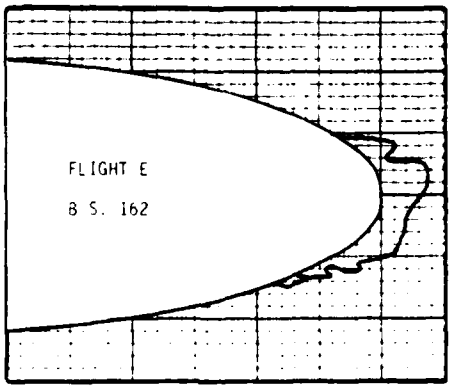

Figure 8. Flight E Ice Shapes From Tracings

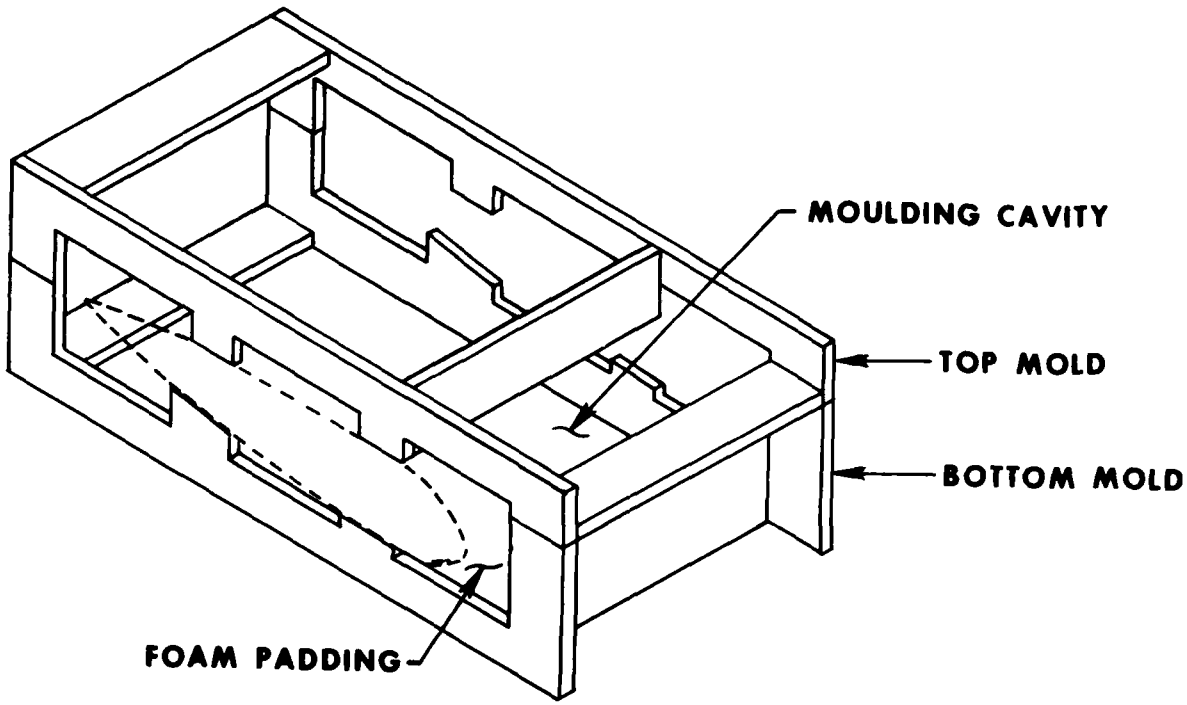

Figure 9. Plywood Mold Frame

The ends of each mold were cut off to assure a clean cross-section. The resulting molds covered approximately 4 inches on the top of the blade, 5 inches on the bottom, and 10 inches in span. Photographs of representative molds are shown in photo 14; and representative cross-sections are shown in photos 15 through 17. The molds produced very accurate ice shape contours, and the molding operation was fully successful.

PROFILE DRAG

24. Ice formation on the rotor blades will increase the profile drag. Before and after accreting ice on every flight, the aircraft was run on the ground at several rotor speeds and zero collective. Main rotor torque was measured, and main rotor power was calculated. Profile power (the power required to pull the blade through the air) varies linearly with the cube of angular velocity. A plot showing density corrected main rotor power versus rotor speed cubed is shown in figure 1, appendix E. Flights C and D are not shown because the main rotor torque instrumentation was inoperative. The data show an increase in profile power at normal rotor speed and sea level standard density of approximately 25 horsepower for the ice accreted in Flight A (0.2 inches at midspan), 45 horsepower in Flight B (0.3 inches), and 60 horsepower in Flight E (0.4 inches).

25. Temperatures for these datum points ranged from -9.5° C to -19° C. Blade tip Mach Numbers ranged from 0.70 (290 rpm at -9.5° C) to 0.79 (324 rpm at -19°C). Part of the profile power can be attributed to compressibility at these relatively high Mach numbers. The power data were corrected for compressibility using a modified form of the Prandtl-Glauert correction (ref 7, app A, and app D), and are shown in figure 2, appendix E. A significant advantage of presenting incompressible power data is that the linear fairing through all data passes through the zero rpm, zero power point. This, in turn, allows Cp_o (profile power coefficient) to be represented by a constant throughout the rpm range. Cp_o is the non-dimensionalized slope of the linear fairings on figure 2. The average profile drag coefficient ($\overline{Cd_o}$) is a linear function of $\underline{Cp_o}$. Details are shown in appendix D. Tabulated values for $\overline{Cd_o}$ and Cp_o are shown in table 2.

26. The measure of profile power and its non-dimensional counterparts showed increasing profile drag with greater ice accretion. The data consistency gives reason for a relatively high confidence level in the data presented.

Photo 12. Pouring Molding Compound Into Frames on Rotor Blade

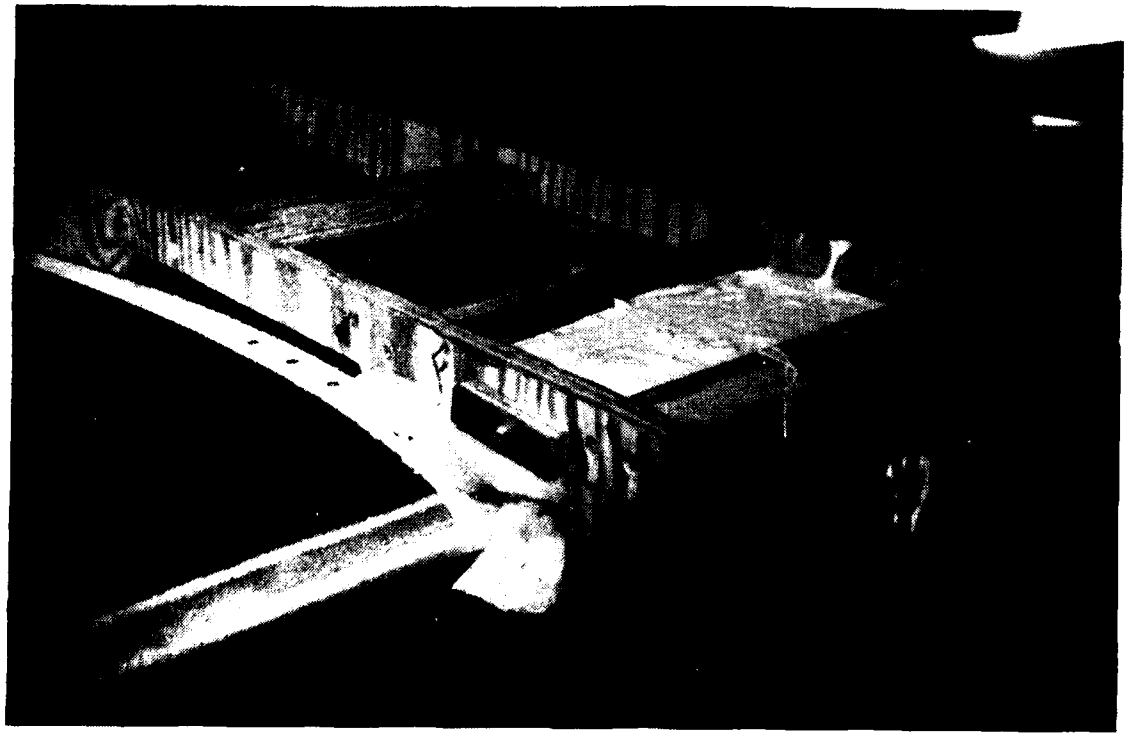

Photo 13. Molding Compound in Plywood Frame

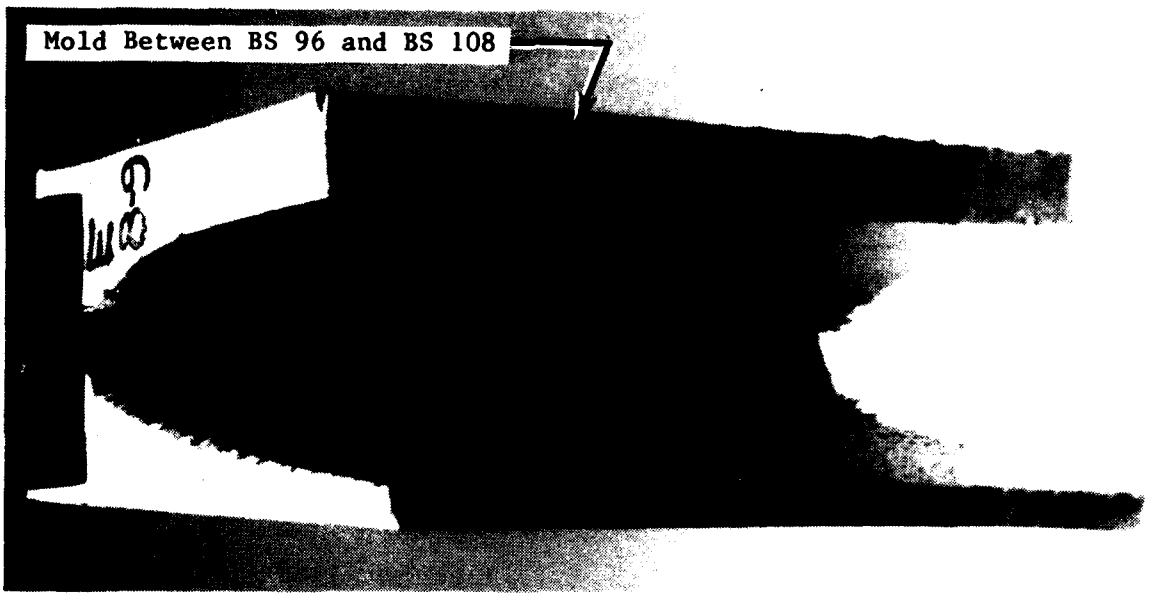

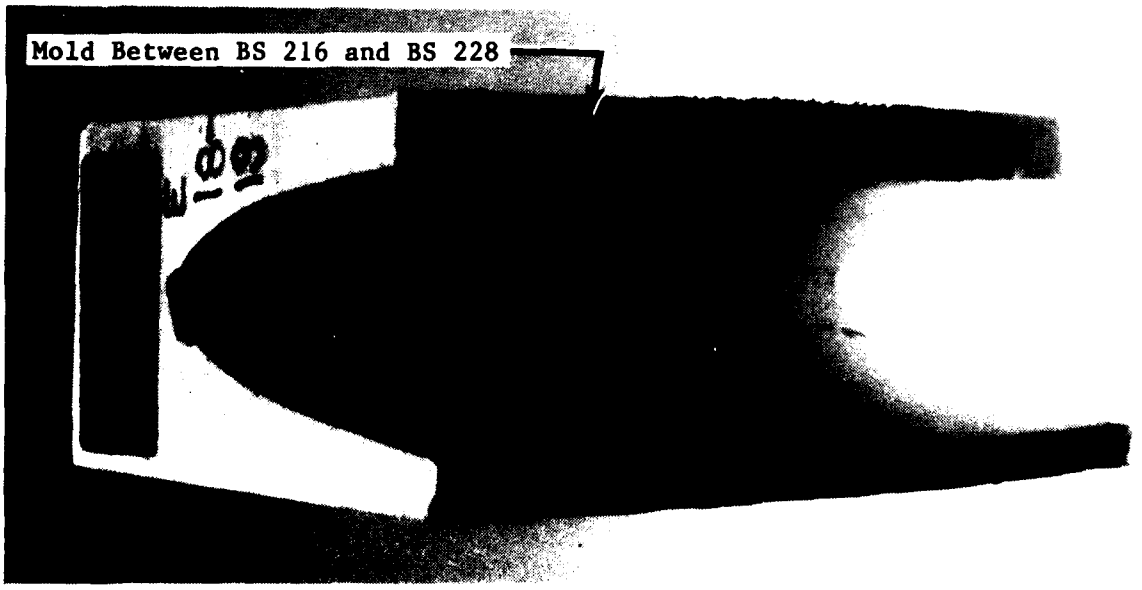

Photo 14. Mold Samples for Flight E

Blade Station 150

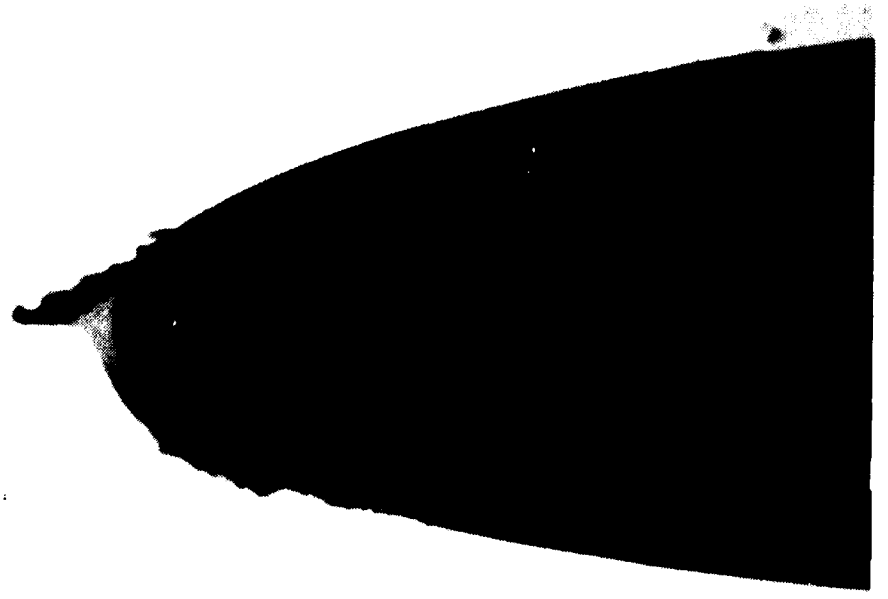

Blade Station 174

Photo 15. Cross Section of Ice Molds from Flight B

Blade Station 126

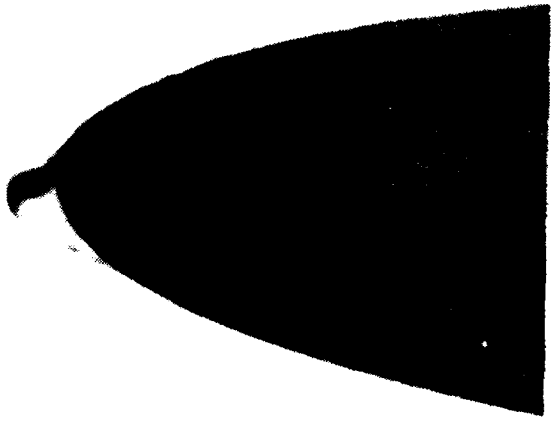

Blade Station 222

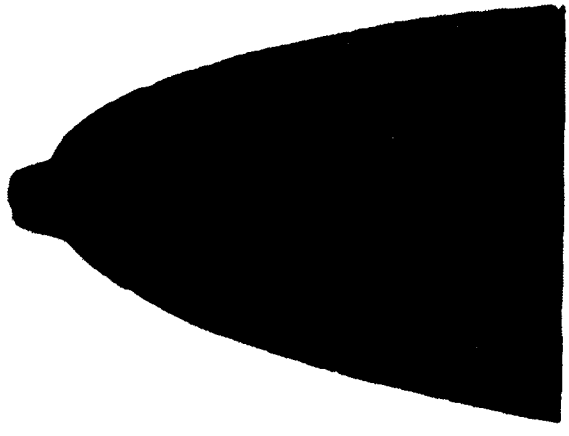

Blade Station 246

Photo 16. Cross Section of Ice Molds from Flight D

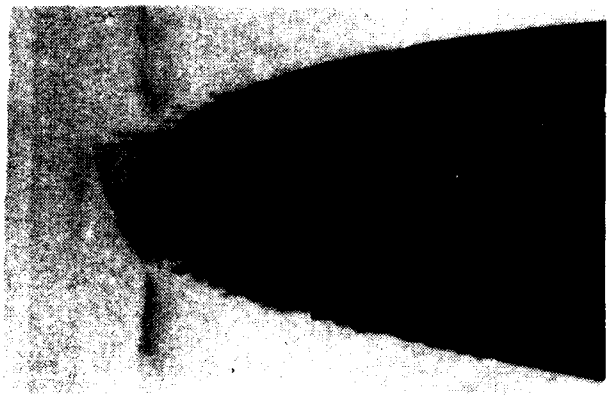

Blade Station 102

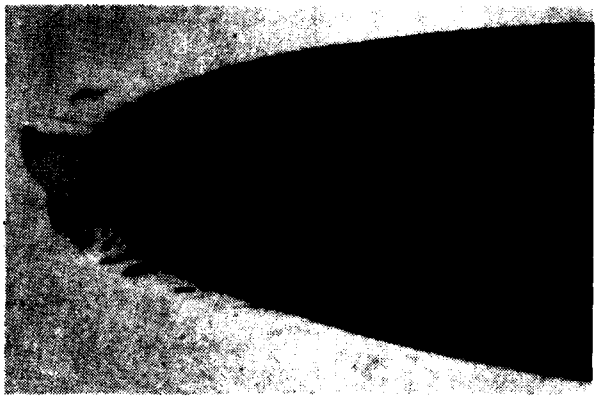

Blade Station 174

Blade Station 126

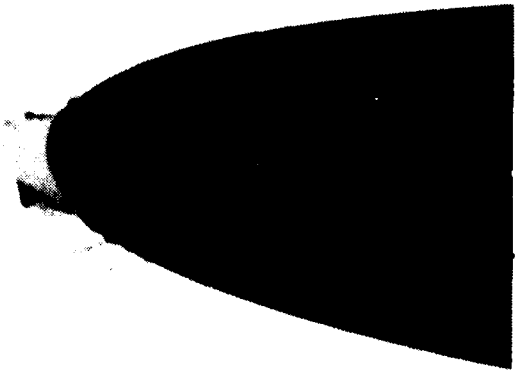

Blade Station 198

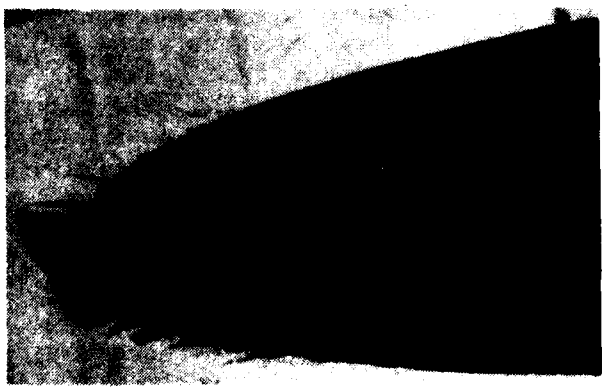

Blade Station 150

Photo 17. Cross Section of Ice Molds from Flight E

Table 2. Incompressible $\overline{Cd_o}$ with Accreted Ice

Flight	Ice Thickness at Mid-Span (inches)	Cp_{o_5} x 10^5	$\overline{Cd_o}$
Baseline	0.0	5.28	.0091
A	0.2	5.75	.0099
B	0.3	6.04	.0104
E	0.4	6.40	.0110

HOVER PEFORMANCE DEGRADATION

27. Tethered hover performance flights were performed at Ottawa and Edwards AFB in winds of less than 2 knots. The data are presented in figure 3, appendix E. The data were compared to previous UH-1H data (ref 8, app A), and matched very closely. The reference 8 hover curve is used on figure 3.

28. Hover performance data for the UH-1H characteristically show scatter. Large quantities of data are gathered to attain a statistically significant curve, which can then be presented with confidence. During these icing tests, a single free hover point was flown before and after each ice accretion. The data (table 3) consistently show greater power required with ice than without ice, but the magnitude of the increase does not correlate with the quantity of ice accreted. The lack of correlation may be caused by normal hover performance data scatter. The best way to obtain hover performance test data with accreted ice is to take a statistically significant number of datum points. However, this cannot be done without shedding the ice during the test. A possible alternative would be to attach imitation ice forms to the blades and then conduct a performance test.

Table 3. Hover Performance Degradation

Flight	Ice Thickness at Mid-Span (inches)	Initial Wind Velocity (knots)	Initial C_T[1] (x 10^4)	Initial C_P[2] (x 10^5)	Wind Velocity after Ice Accretion (knots)	C_T after Ice Accretion (x 10^4)	C_P after Ice Accretion (x 10^5)	Cp after Ice Accretion at Initial C_T[3] (x 10^5)	ΔC_P	Equivalent (Standard Day) Power Change (shp)
A	0.2	7	25.2	16.2	7	25.2	18.6	18.6	2.4	+101
B	0.3	8	23.6	15.6	7	23.2	16.5	16.8	1.2	+ 50
C	not measured	8	24.3	17.1	7	24.3	18.3	18.3	1.2	+ 51
D	0.2	0	24.3	16.4	8	23.9	17.5	17.8	1.4	+ 60
E	0.4	7	22.3	15.0	8	22.5	17.3	17.1	2.1	+ 89

NOTES:

[1] C_T = Thrust coefficient
[2] C_P = Power coefficient

3: $\dfrac{dC_P\ (\times 10^5)}{dC_T\ (\times 10^4)} = 0.85$

LOW SPEED FLIGHT PERFORMANCE

29. Low speed performance was evaluated at Edwards AFB after conclusion of the Ottawa testing to correlate hover in winds data. Two methods of testing were used: tethered hover in known winds (figs. 4 through 6, app E) and low speed pace at several weights (figs. 7 through 13). The data show decreasing power required with increasing speed (or wind). Performance summaries are presented in figure 14.

30. The data in figures 3 through 14 were analyzed using a standard thrust coefficient (C_T), power coefficient (C_P), advance ratio (μ) carpet plotting technique. An alternate technique (GENFLT) presented in reference 9, appendix A eliminates C_T as an independent variable and relates power required to hover power required and nondimensional forward flight velocity. The data in figures 7 through 13, appendix E is presented in GENFLT format in figure 10 of this text.

FIGURE 18
GENERALIZED LOW SPEED PERFORMANCE

$CPG=(C_P-C_{P_h})/.707C_T^{3/2}$

WHERE C_{P_h} IS FROM HOVER CURVE

$\bar{V}_h = \mu/\sqrt{C_T/2}$

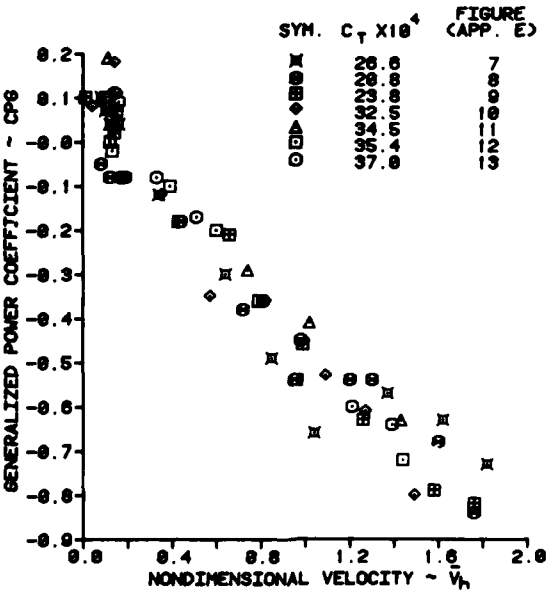

CONCLUSIONS

31. Tethered hover testing causes shedding of accreted ice (para 8).

32. Adequate ice formation could not be retained at ambient temperatures above -9.5°C (para 10).

33. All ice documentation methods: steroscopic photography, tracings, and molds, worked well and provided accurate ice contours. (paras 19, 20, and 23).

34. Changes in profile power caused by rotor icing could be measured consistantly during ground runs, and was the most valuable indicator of performance loss (para 26).

35. Performance degradation caused by rotor icing in a hover could not be correlated with quantity and accreted ice using a single free hover point (para 28).

35. Hover performance degradation data must be gathered in sufficient quantities to be statistically significant (para 28).

36. Low speed performance data were obtained (para 29).

APPENDIX A. REFERENCES

1. Letter, AVRADCOM, DRDAV-DI, 18 October 1982, subject: Evaluation of UH-1H Hover Performance Degradation Due to Rotor Icing, Test Request No. 82-12.

2. Test Plan, USAAEFA Project No. 82-12, *Evaluation of UH-1H Hover Performance Degradation Caused by Rotor Icing,* November 1982.

3. Technical Manual, TM 55-1520-210-10, *Operator's Manual, Army Models UH-1D/H Helicopters,* 18 May 1979.

4. National Research Council of Canada Aeronautical Report LR-186A, *Description of the Spray Rig Used to Study Icing on Helicopters in Flight,* September 1960.

5. Paper, Palko, R.L. and Cassady, P.L., "Photogrammetric Development and Application at AEDC", AIAA Paper No. 82-0610 presented at AIAA Twelfth Aerodynamic Testing Conference, Williamsburg, Virginia, March 1982.

6. Technical Report, AEDC TR-83-43, Palko, R.L. and Cassady, P.L., *Photogrammetric Analysis of Ice Buildup on a US Army UH-1H Helicopter Main Rotor in Hover Flight,* to be published.

7. Shapiro, Ascher H., *The Dynamics and Thermodynamics of Compressible Fluid Flow,* Ronald Press Co., New York, 1953.

8. Final Report, USAASTA Project No. 66-04, *Engineering Flight Test YUH-1H Helicopter,* November 1970.

9. Paper, Boirun, B.H., "Generalizing Helicopter Flight Test Performance Data (GENFLT)", AHS Preprint No. 78-44 presented at the 34th Annual National Forum of the American Helicopter Society, Washington, D.C., May 1978.

APPENDIX B. NATIONAL RESEARCH COUNCIL ICING SPRAY RIG DESCRIPTION

ICING SPRAY RIG DESCRIPTION

1. The National Research Council icing spray rig is located adjacent to Canadian Forces Base Uplands in Ottawa, Canada. It consists of a welded steel framework supporting a 75 ft wide by 15 ft tall spray nozzle array attached to a 59 ft tall mast (photos 1 and 2). The array may be rotated ±180° about the mast for alignment into the wind. An electric winch raises and lowers the array on the mast, and the spray rig can be operated in either the full up or full down position (top of the array 54 and 24 feet from the ground, respectively). A cup anemometer is attached on top of the framework for windspeed measurement.

2. The array contains a total of 156 steam atomizing nozzles mounted 3 feet apart on 30 vertical bars (photos 3 and 4). The nozzles use pressurized steam to atomize the water into a spray cloud. Liquid water content (LWC) is determined by water flow rate and windspeed, and drop size is governed by steam pressure. A median volumetric drop diameter of 30 microns was the aim condition for these tests.

3. The test procedure consists of hovering the aircraft 20 to 30 ft above the ground at a nominal standoff distance of 100 ft from the spray rig, and allowing the wind to carry the spray cloud from the array into the rotor system. The cloud entry technique was to first establish a hover outside the cloud, and then transition into the cloud from the side. Winds of at least 6 knots are required to properly develop the cloud for tests with a UH-1 sized aircraft. At windspeeds below this, the aircraft rotor wash prevents the cloud from effectively entering the rotor system. Photos 5 and 6 illustrate the difference in cloud formation between adequate wind conditions and insufficient winds.

4. Figures 1 and 2 give the calculated nozzle spray performance in terms of LWC and drop size for varying windspeeds, water flows, and steam pressues. These are the figures used by the spray rig control room to establish flow settings for the desired test condition. Wind speed and gustiness impact uniformity of the cloud and affect estimation of LWC. Consistency of rotor immersion during a test is affected by changes in wind direction and gustiness, which move the cloud relative to the aircraft. Figure 2 shows the empirical gustiness correction factor used to adjust water flow rate to compensate for LWC differences in the spray cloud between the spray array location and the test aircraft. This correction factor was determined empirically by the NRC from icing test results of a Bell-47J helicopter where the measured ice thickness on the rotor blades was correlated to calculated

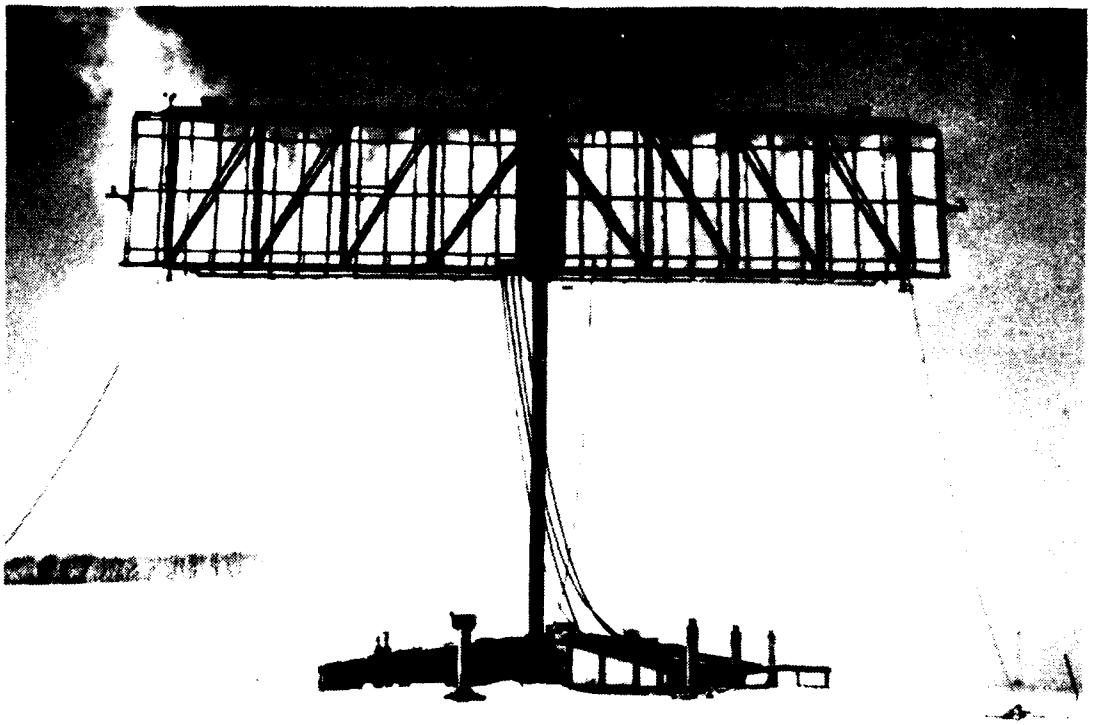

Photo 1. NRC Icing Spray Rig in the Fully Raised Position

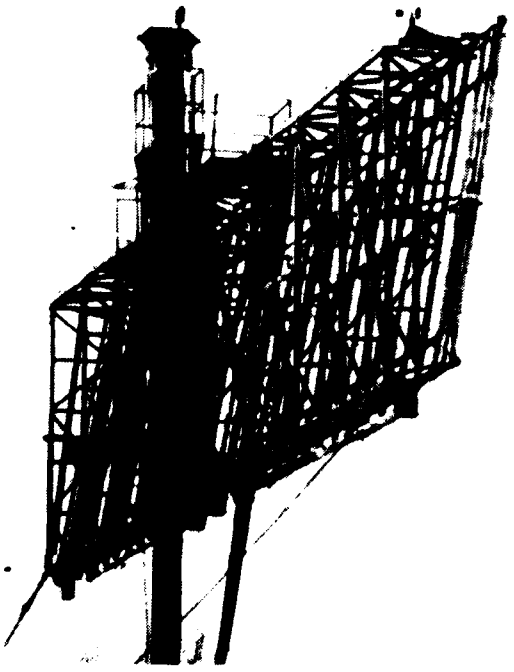

Photo 2. Icing Spray Rig Framework, Nozzle, Venting Steam (No Water) at an "Idle" Setting

Photo 3. Steam Atomizing Nozzle Installed on the Spray Rig

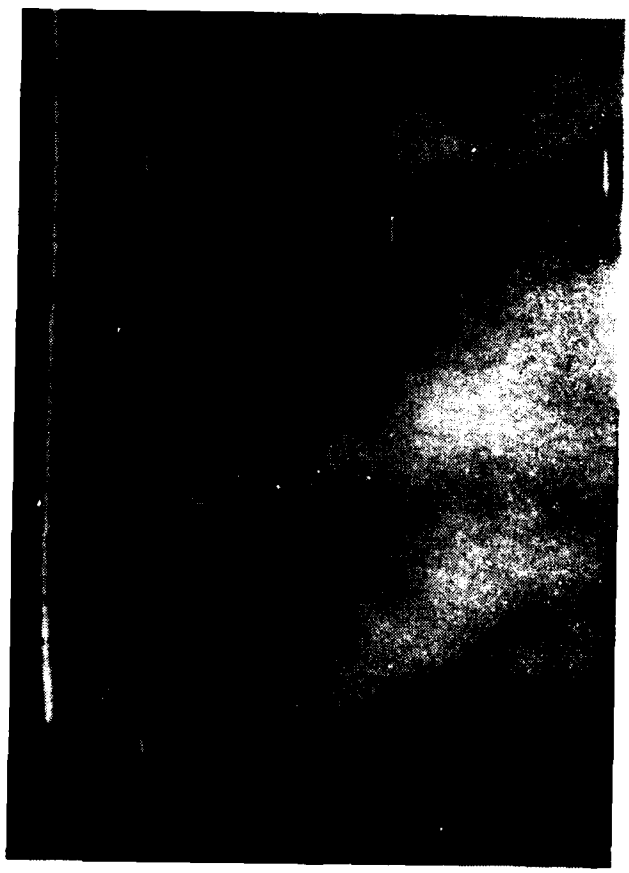

Photo 4. Vertical Bars Supporting the Spray Nozzle

Photo 5. Spray Cloud Properly Developed with 9 KTAS Wind for Immersion of UH-1H Rotor System

Photo 6. Insufficient Winds (Below 6 KTAS) to Properly Move the Spray Cloud Onto the Rotor System

values of LWC. The maximum water flow rate available is 6200 lbs/hr, which reduces the maximum attainable LWC below 0.9 gm/m^3 under some conditions.

5. The charts in figures 1 and 2 are used by first obtaining the LWC correction factor (fig. 2) which corresponds to the existing wind conditions. The LWC at the spray array is then computed by multiplying the required test LWC by the correction factor. Water flow and steam pressure are then determined using figure 1.

FIGURE 1 DETERMINATION OF ICING SPRAY RIG LWC

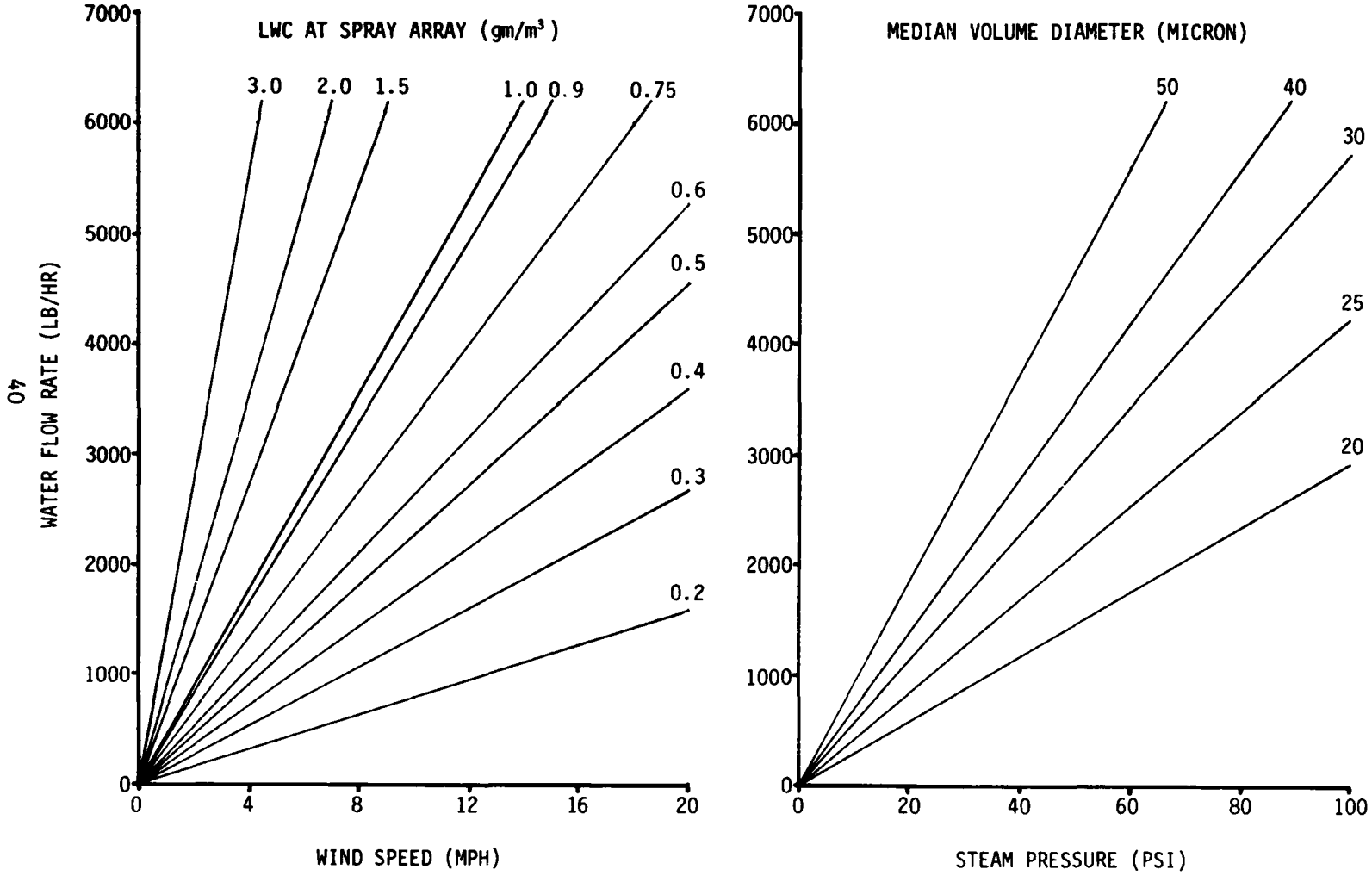

FIGURE 2 CORRECTION FACTOR TO BE APPLIED TO CALCULATED LWC

NOTES: 1. HELICOPTER 100 FT FROM SPRAY ARRAY
2. LWC AT SPRAY ARRAY = (REQUIRED TEST LWC) X (LWC CORRECTION FACTOR)
3. GUSTINESS: LOW = 0 TO ± 1½ MPH
MEDIUM = ± 1½ TO ± 3 MPH
HIGH = ± 3 MPH OR HIGHER

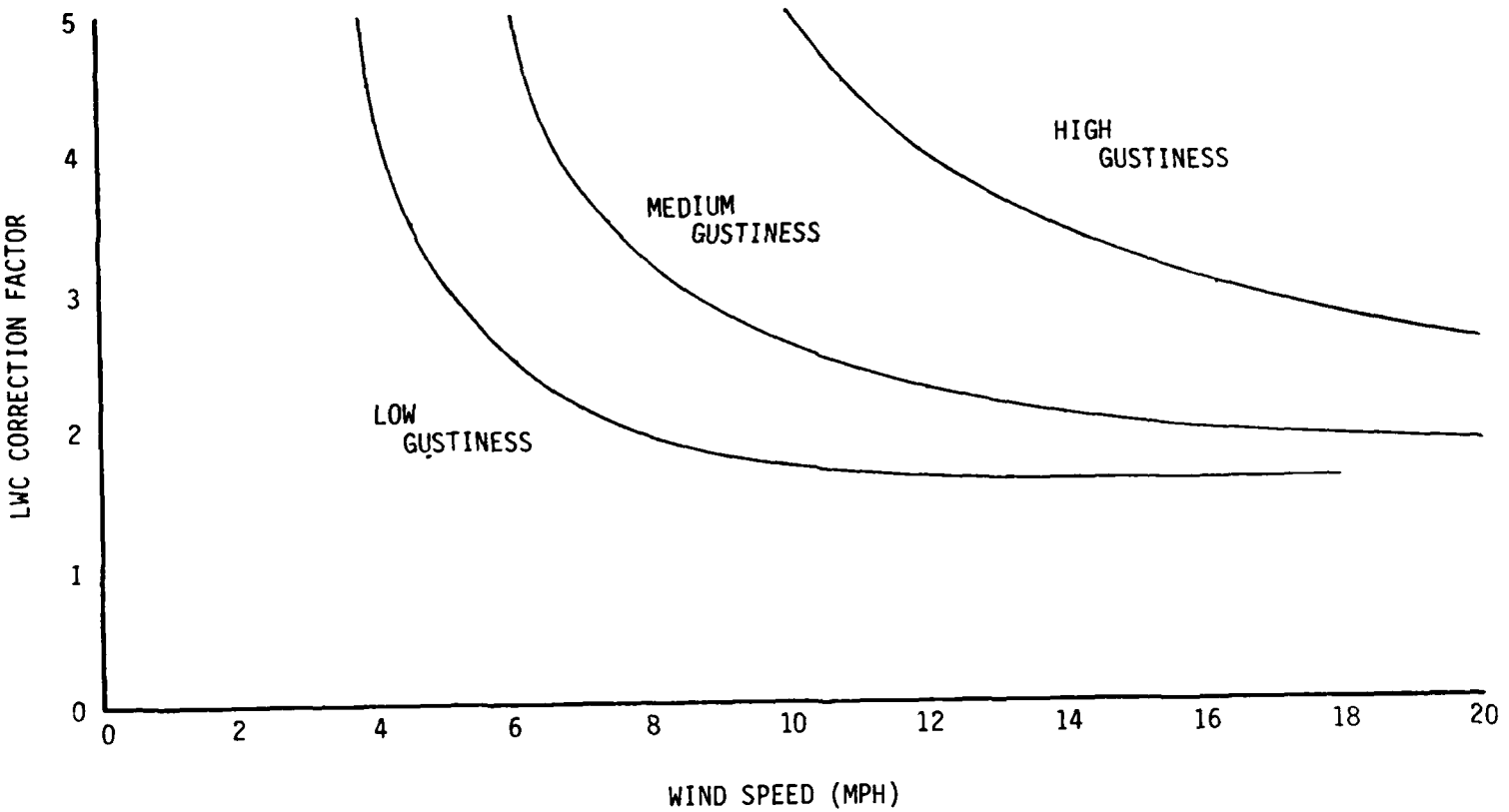

APPENDIX C. INSTRUMENTATION

1. Except for the main rotor blade load instrumentation, the test instrumentation was installed, calibrated, and maintained by US Army Aviation Engineering Flight Activity (USAAEFA) personnel. Digital and analog data were obtained from calibrated instrumentation and were recorded on magnetic tape and/or displayed in the cockpit. Recorded data were taken at 10 samples per second, and 5 Hz filters were used. Blade and mast instrumentation was installed by Bell Helicopter Textron.

2. The test instruments displayed in the cockpit are listed below.

Main rotor speed
Engine torque
Pressure altitude
Engine inlet differential pressure
Load cell
Outside air temperature
Fuel used
Control positions (4)
Time of day
Run number

3. Data parameters recorded onboard the aircraft in PCM format are listed below.

Time of day
Event
Run number
Main rotor speed
Main rotor torque
Engine torque
Turbine speed
Compressor speed
Liner acceleration (3)
Fuel used
Magnetic heading
Pressure altitude
Outside air temperature
Measured gas temperature
Control positions (4)
Fuel temperature
Roll attitude
Pitch attitude
Attitude rates (3)
Blade flapping
Blade pitch
Pitch link load

Mast parallel bending
Mast perpendicular bending
Hub beam and chord bending
Blade beam and chord bending (B.S. 35)
Blade beam and chord bending (B.S. 84)
Blade beam and chord bending (B.S. 150)
Blade beam and chord bending (B.S. 192)
Blade beam and chord bending (B.S. 234)

4. The following were recorded on the ground.

Ambient temperature
Ambient pressure
Wind speed and direction
Water flow rate (spray rig)
Steam and water pressures (spray rig)

APPENDIX D. DATA ANALYSIS METHODS

SPRAY RIG DATA

1. Cloud data, including liquid water content (LWC), was obtained from NRC tables shown in appendix B. LWC was determined empirically by a combination of water flow rate, wind velocity, and wind gustiness.

AIRCRAFT WEIGHT AND BALANCE

2. Prior to testing, the aircraft weight and center of gravity location were determined with calibrated scales. The aircraft was weighed in the instrumented configuration with full oil and trapped fuel on board.

3. Fuel quantity was measured pre and post flight using a sight gage calibrated during previous testing. The fuel weight for each test was determined prior to flight by using the external sight gage to measure volume, and a hydrometer to measure specific gravity.

4. Aircraft weight was determined in flight using known takeoff weight and the fuel volume used instrumentation. This instrumentation calibration was performed in the laboratory and verified and modified by comparing the fuel used indication with the sight gage readings.

5. During tethered hover, a calibrated load cell was used to measure thrust in excess of aircraft weight. Load cell tare readings were recorded before and after each flight.

NONDIMENSIONAL PARAMETERS

6. Nondimensional parameters were used to normalize speed, thrust and power. Speed was nondimensionalized as advance ratio (μ), thrust as thrust coefficient (C_T) and power as power coefficient (C_P).

$$\mu = \frac{V_T}{\mu R} \tag{1}$$

$$C_T = \frac{\text{Thrust}}{\rho A(\Omega R)^2} \tag{2}$$

$$C_P = \frac{\text{Power}}{\rho A(\Omega R)^3} \qquad (3)$$

where:

V_T = vector sum of wind speed and speed of aircraft relative to earth (ft/sec)

Ω = angular velocity of the main rotor (radians/sec)

R = main rotor radius (24 feet)

Thrust = aircraft weight plus any tethered load (pounds)

A = main rotor area (1809 ft^2)

Power = engine power for C_P, main rotor mast power for C_{P_o} (ft-lb/sec or 550 x horsepower)

ρ = density of air (slugs/ft^3) measured by using ambient temperature (°C) and pressure (inches of mercury)

$$\rho = .0023769 \times \frac{\text{pressure}}{29.92} \times \frac{288.15}{\text{temperature} + 273.15}$$

Pressure = ambient pressure (inches of mercury)
Temperature = ambient temperature (degrees C)

COMPRESSIBILITY CORRECTION

7. Profile power is that power required to pull the blade through the air. Profile power is composed of incompressible profile power and a power component due to compressibility. It was desired to remove the compressible portion of profile power from the total (measured) power and study incompressible profile power. The following Prandtl-Glauert equation was used:

$$P_{inc} = P\,[1-(.75\ M_{tip})^2]^{1/2} \qquad (4)$$

The equation uses the .75 blade radius as the representative station for analysis.

DRAG COEFFICIENT

8. A mean profile drag coefficient ($\overline{Cd_o}$) can be developed from blade element considerations if the section profile drag coefficient is assumed constant along the blade span.

$$\overline{Cd_o} = \frac{8\ Cp_o}{\sigma} \qquad (5)$$

Where:

σ = Solidity ratio (0.0464)

HOVER AND LOW SPEED PERFORMANCE

9. The C_P, C_T, and μ data gathered during tethered hover and low speed flight were plotted aganist one another using a standard carpet plotting technique. Consistant families of curves were faired through the data in both dimensions (C_P vs C_T, and C_P vs μ).

APPENDIX E. TEST DATA

INDEX

FIGURE 1

PROFILE POWER AT ZERO COLLECTIVE

UH-1H USA S/N 69-15532

SYMBOL	FLIGHT	DENSITY ALTITUDE (FEET)	OAT (DEG C)	ICE THICKNESS AT MID-SPAN (INCHES)
⊖	A	-2560	-12.0	0.2
△	B	-2580	- 9.5	0.3
⊡	E	-4620	-19.0	0.4

NOTE: 1) OPEN SYMBOLS DENOTE CLEAN BLADES.
CLOSED SYMBOLS DENOTE ICED CONDITIONS.

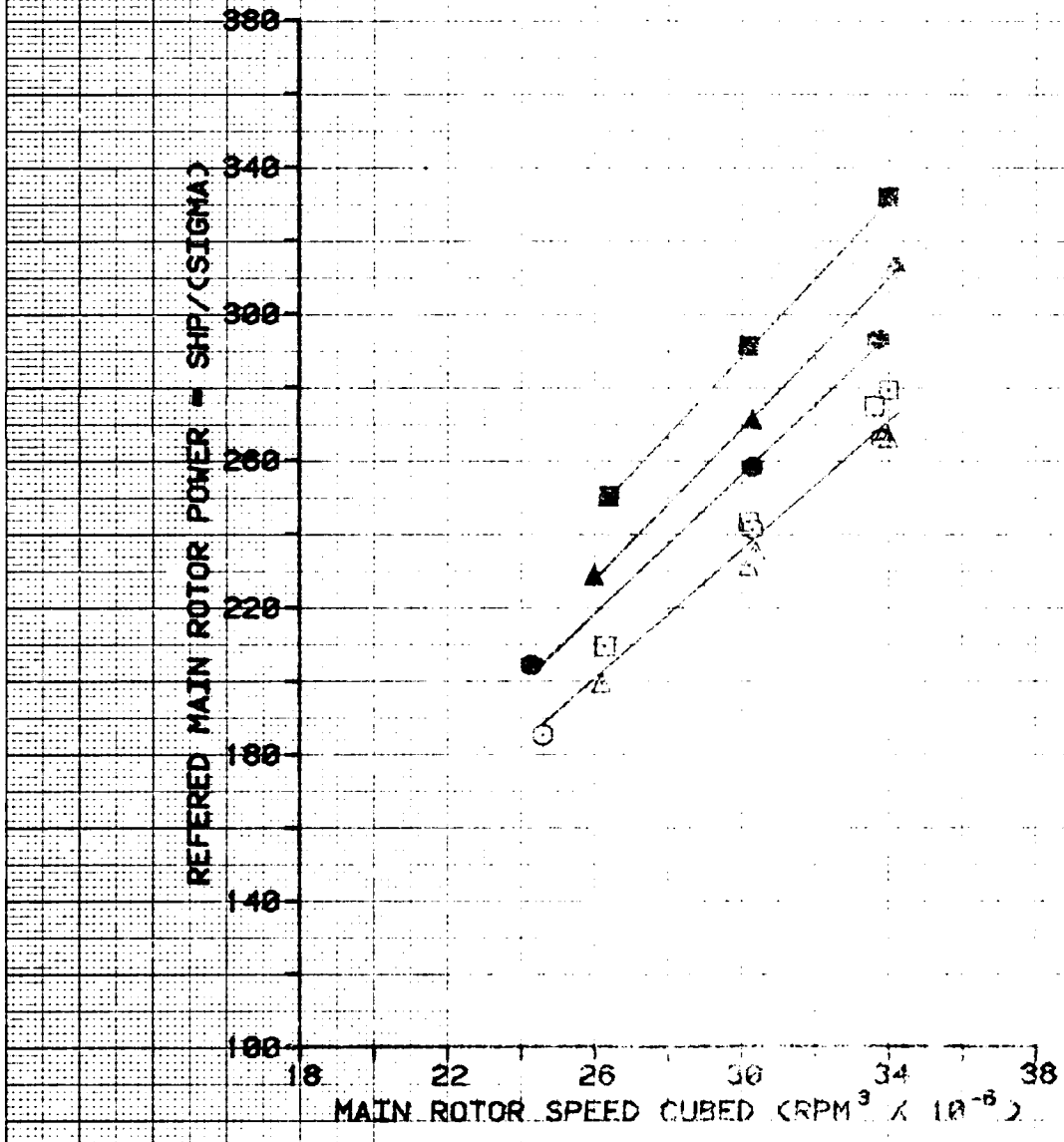

INCOMPRESSIBLE PERFORMANCE OF [illegible] ROTOR IN HOVER AT [illegible] EFFECTIVE BLADE-TIP MACH NUMBER

SYMBOL	FLIGHT	DENSITY ALTITUDE (FEET)	OAT (DEG C)	ICE THICKNESS AT RED-SPAN (INCHES)
○	A	[illegible]	-12.6	0.2
□	B	[illegible]	-8.3	0.3
△	E	[illegible]	-19.0	0.4

NOTES: 1) OPEN SYMBOLS DENOTE CLEAN BLADES.
CLOSED SYMBOLS DENOTE ICED CONDITIONS.
2) CORRECTION FOR COMPRESSIBILITY:

$$\frac{P_{INS}}{P} = [1 - 0.25M_{tip}^2]^{1/2}$$

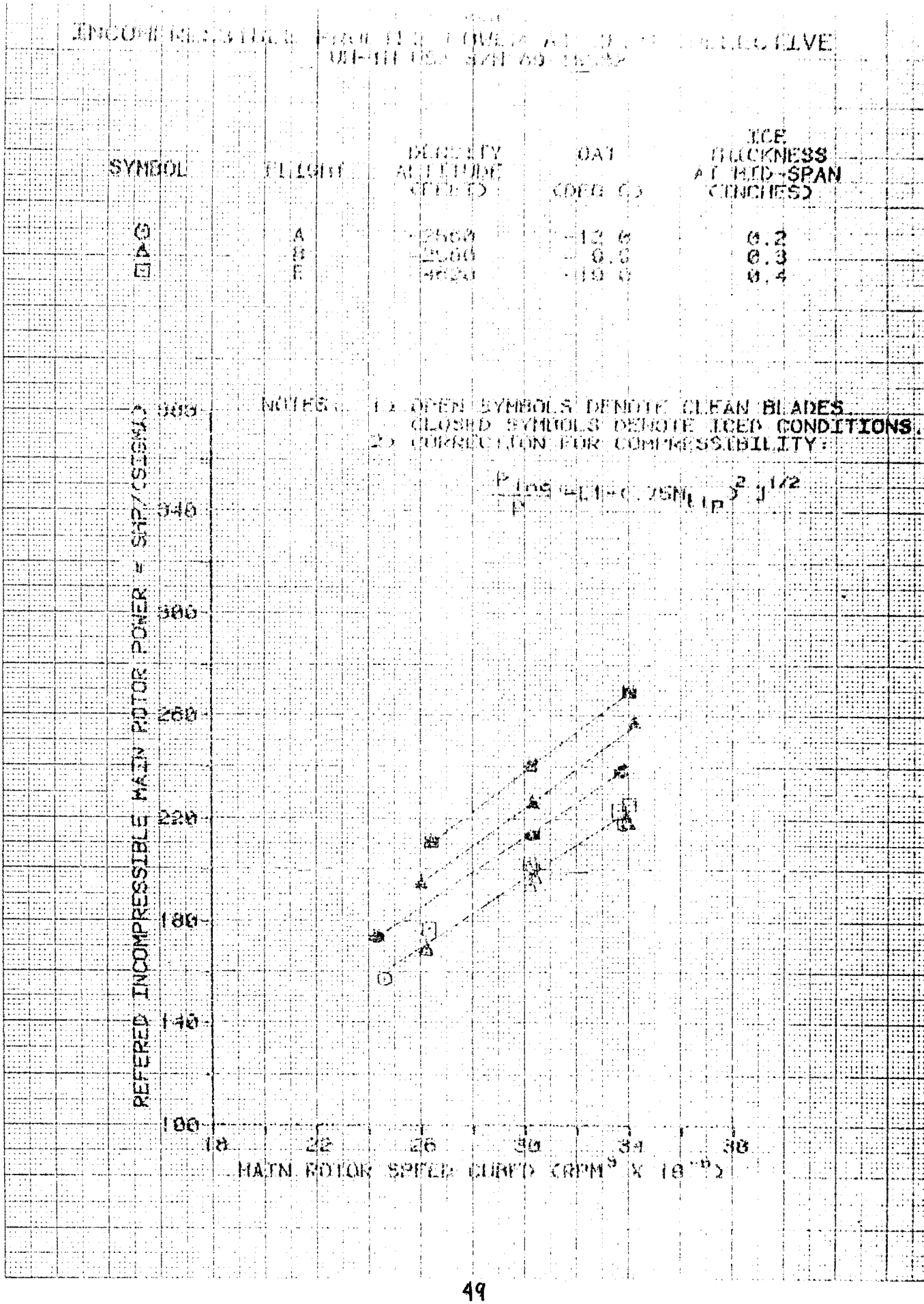

FIGURE 3

NON-DIMENSIONAL HOVER PERFORMANCE

UH-1H USA S/N 69-15532

SYMBOL	AVG DENSITY ALTITUDE (FEET)	AVG ROTOR SPEED (RPM)	AVG OAT (DEG C)
⊙	1580	324	-2.0
◇	1500	315	-2.0
□	4290	321	28.0
△	4290	314	28.0

NOTES:
1) TETHERED HOVER METHOD.
2) SKID HEIGHT 50 FEET.
3) SOLID PORTION OF CURVE TAKEN FROM REFERENCE 8.
4) WINDS LESS THAN 2 KNOTS.

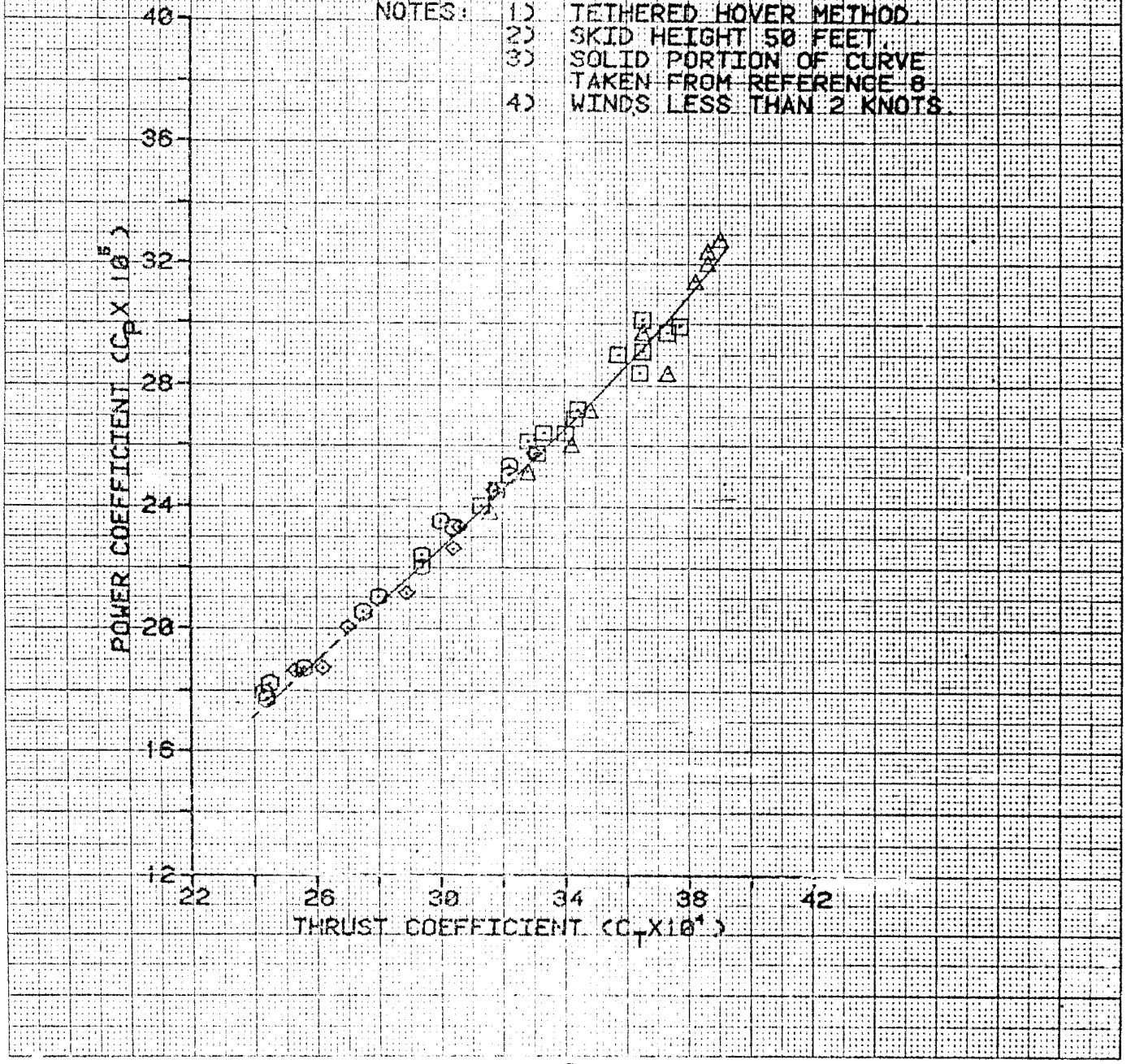

FIGURE 4

NON-DIMENSIONAL LOW-SPEED PERFORMANCE

UH-1H USA S/N 69-15532

SYMBOL	AVG ROTOR SPEED (RPM)	AVG DENSITY ALTITUDE (FEET)	AVG OAT (DEG C)	ADVANCE RATIO
⊡	323	4000	25.0	0.005
△	313	4000	25.0	0.005

NOTES: 1) TETHERED HOVER METHOD.
2) SKID HEIGHT 50 FEET.

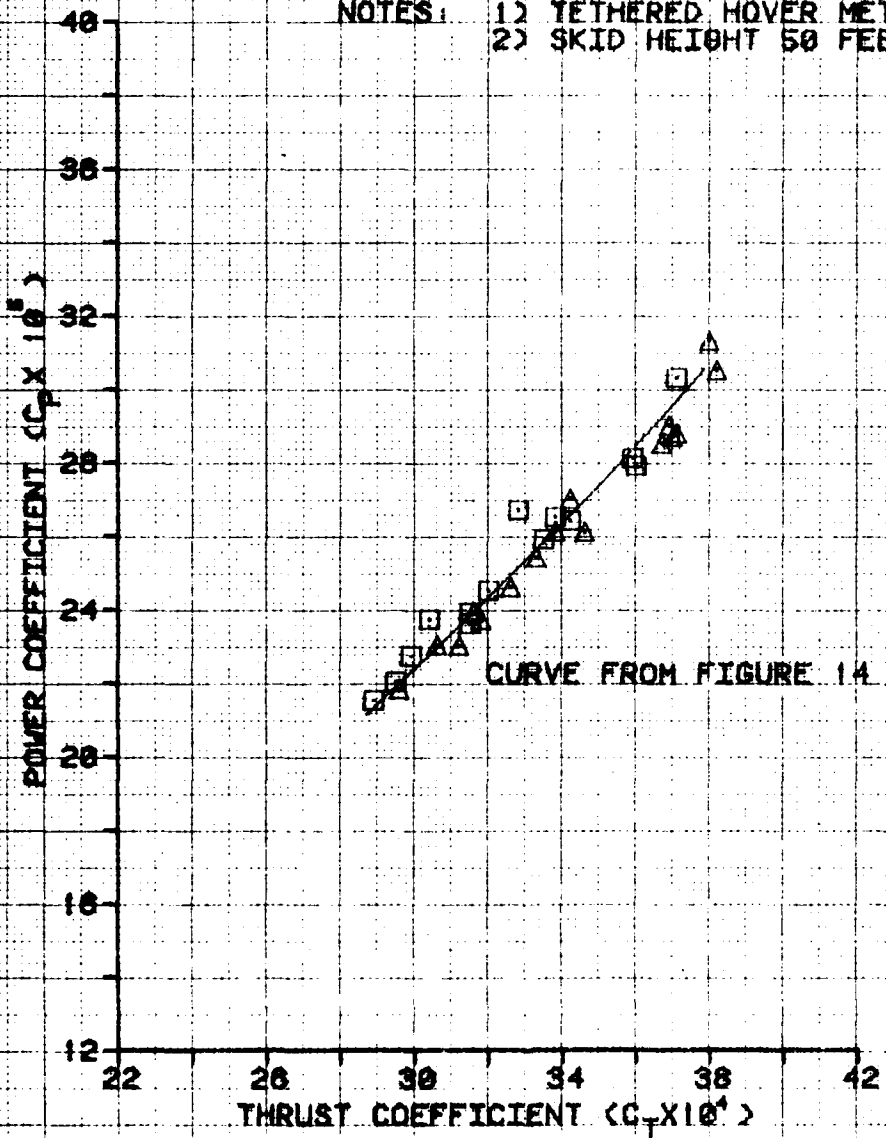

FIGURE 5

NON-DIMENSIONAL LOW-SPEED PERFORMANCE

UH-1H USA S/N 69-15532

SYMBOL	AVG ROTOR SPEED (RPM)	AVG DENSITY ALTITUDE (FEET)	AVG OAT (DEG C)	ADVANCE RATIO
□	324	4120	27.0	0.009
△	314	4120	27.0	0.009

NOTES: 1) TETHERED HOVER METHOD
2) SKID HEIGHT 50 FEET

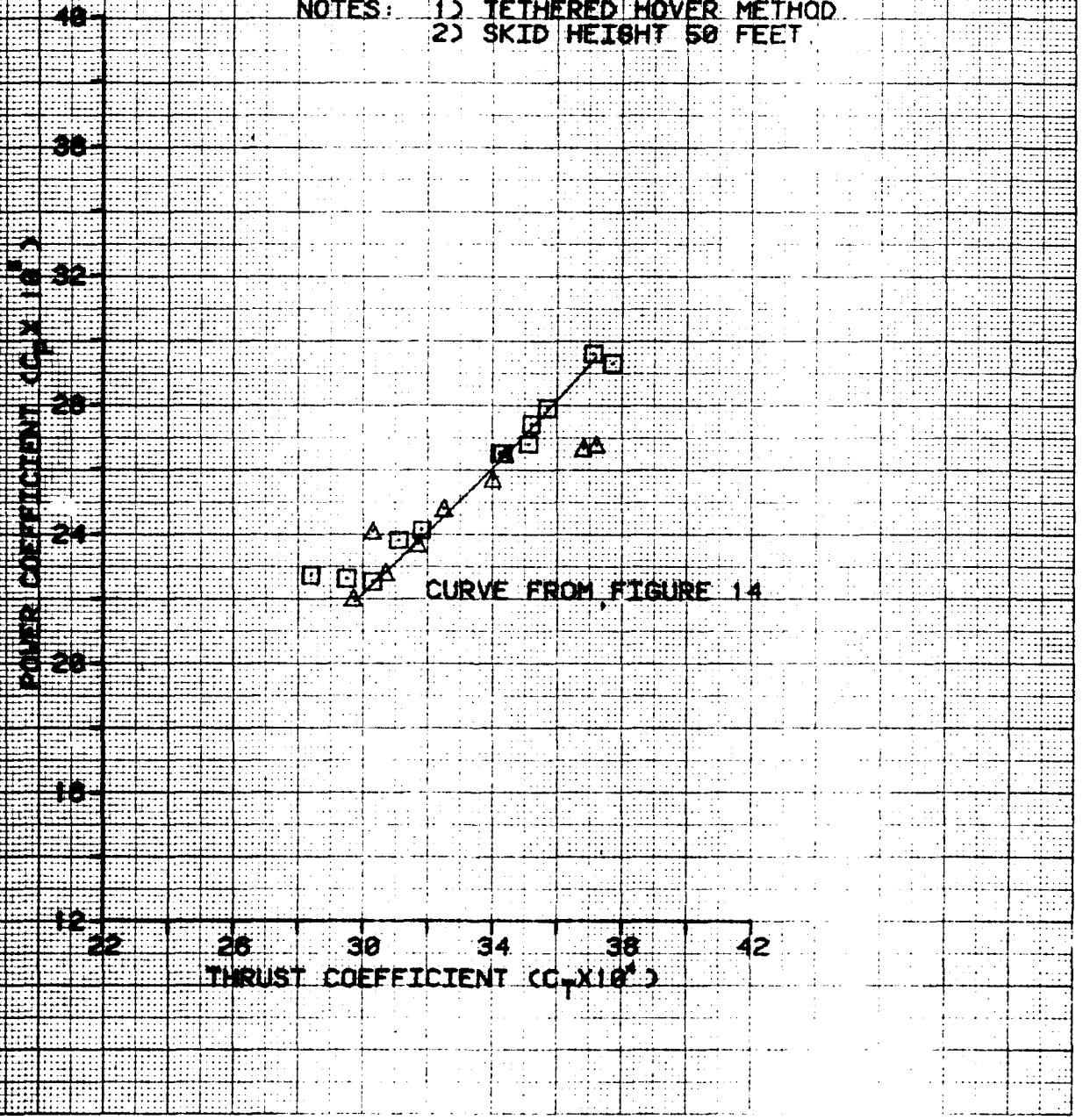

FIGURE 6

NON-DIMENSIONAL LOW-SPEED PERFORMANCE

UH-1H USA S/N 69-15532

SYMBOL	AVG ROTOR SPEED (RPM)	AVG DENSITY ALTITUDE (FEET)	AVG OAT (DEG C)	ADVANCE RATIO
□	324	3000	17.0	0.014
△	313	3000	17.0	0.014

NOTES: 1) TETHERED HOVER METHODS.
2) SKID HEIGHT 50 FEET.

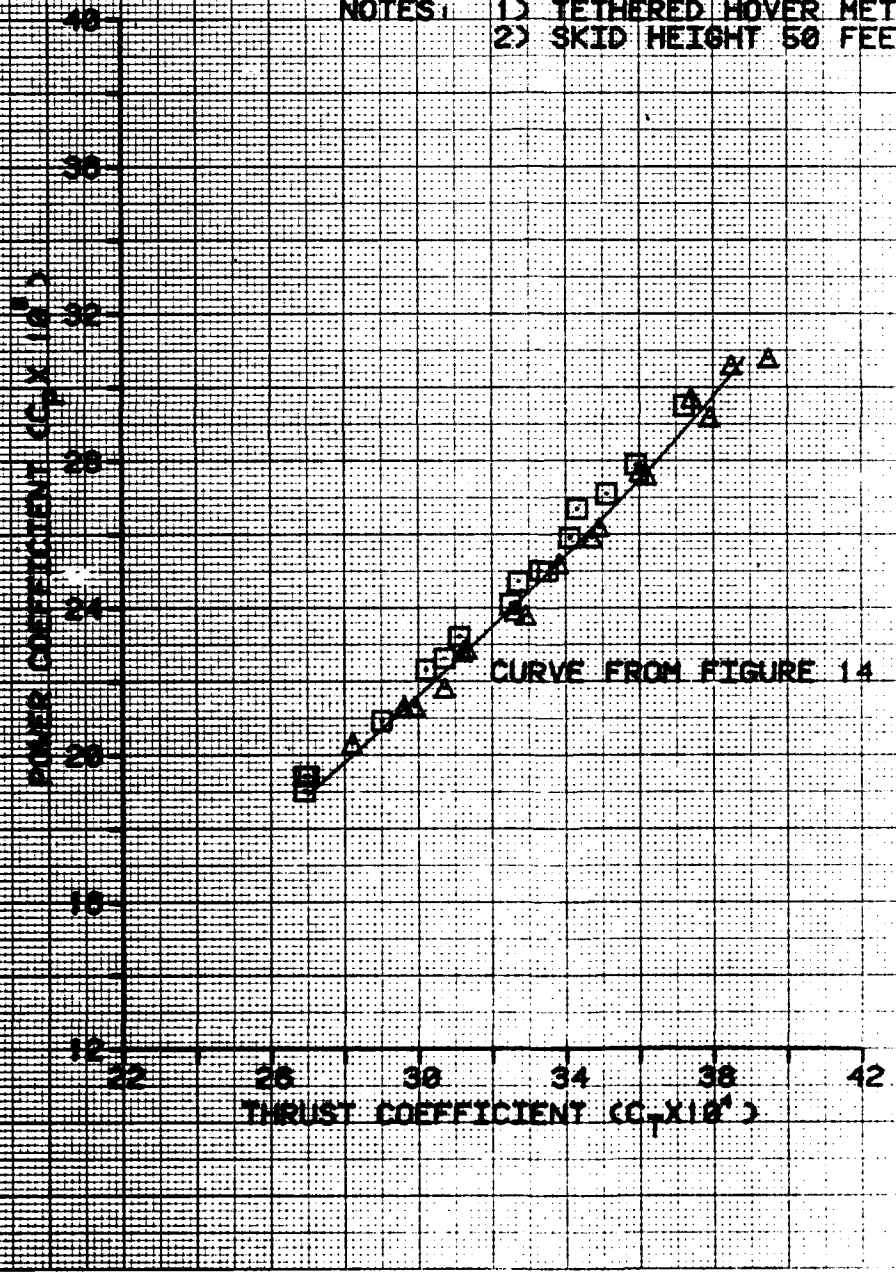

FIGURE 7

NON-DIMENSIONAL LOW-SPEED PERFORMANCE

UH-1H USA S/N 69-15592

SYMBOL	AVG ROTOR SPEED (RPM)	AVG DENSITY ALTITUDE (FEET)	AVG OAT (DEG C)	AVG THRUST COEFFICIENT ($C_T X 10^4$)
⊡	322	3000	19.5	20.6

NOTES: 1) SKID HEIGHT 50 FEET.
2) GROUND VEHICLE PACE.

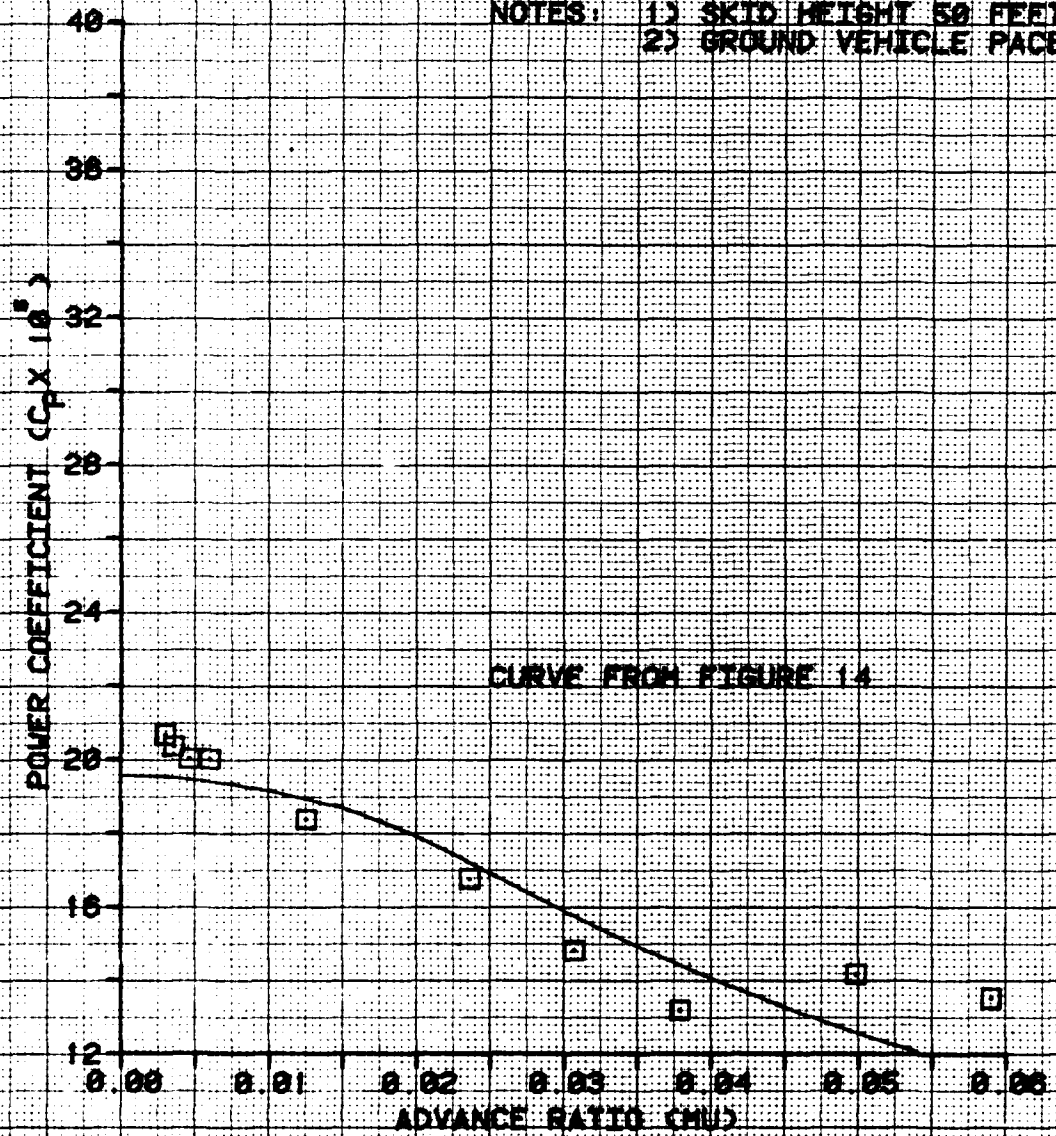

FIGURE 8

NON-DIMENSIONAL LOW-SPEED PERFORMANCE

UH-1H USA S/N 69-15532

SYMBOL	AVG ROTOR SPEED (RPM)	AVG DENSITY ALTITUDE (FEET)	AVG OAT (DEG C)	AVG THRUST COEFFICIENT ($C_T \times 10^4$)
⊡	311	3040	22.0	28.1

NOTES: 1) SKID HEIGHT 50 FEET.
2) GROUND VEHICLE PACE.

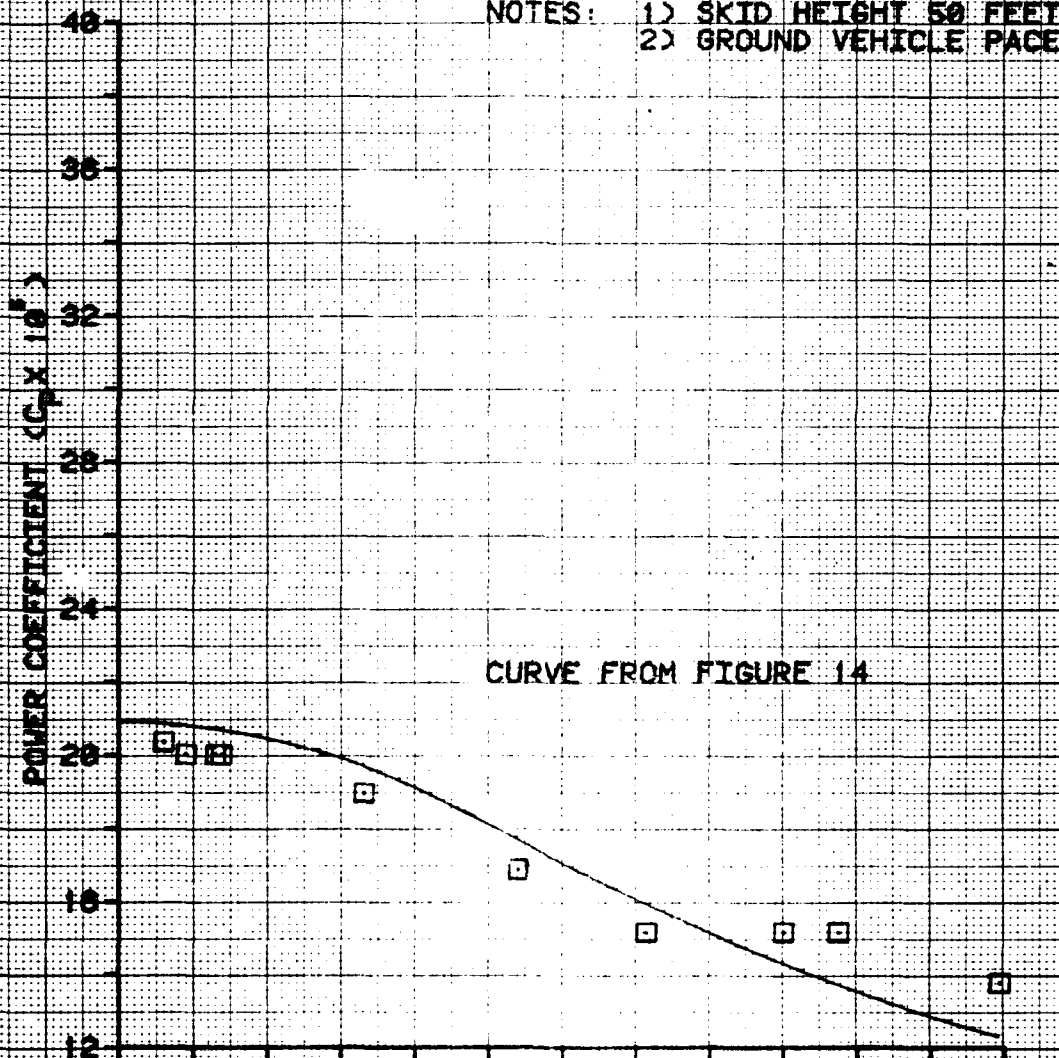

FIGURE 8

NON-DIMENSIONAL LOW-SPEED PERFORMANCE

UH-1H USA S/N 69-15532

SYMBOL	AVG ROTOR SPEED (RPM)	AVG DENSITY ALTITUDE (FEET)	AVG OAT (DEG C)	AVG THRUST COEFFICIENT ($C_T X 10^4$)
⊡	311	2980	18.0	31.3

NOTES: 1) SKID HEIGHT 50 FEET.
2) GROUND VEHICLE PACE.

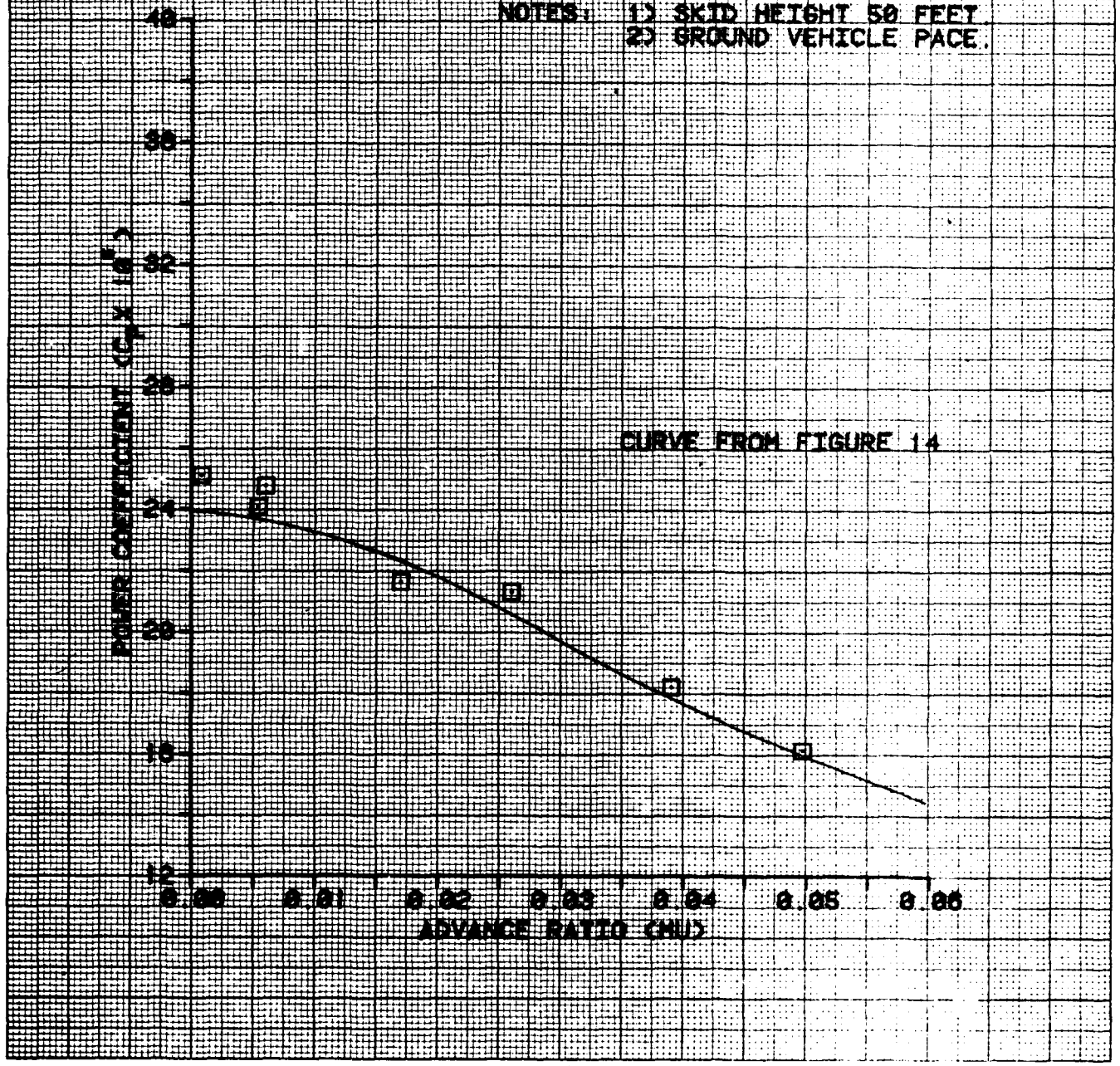

FIGURE 10

NON-DIMENSIONAL LOW-SPEED PERFORMANCE

UH-1H USA S/N 69-15532

SYMBOL	AVG ROTOR SPEED (RPM)	AVG DENSITY ALTITUDE (FEET)	AVG OAT (DEG C)	AVG THRUST COEFFICIENT ($C_T X 10^4$)
⊡	322	2750	15.0	32.5

NOTES: 1) SKID HEIGHT 50 FEET
2) GROUND VEHICLE PACE

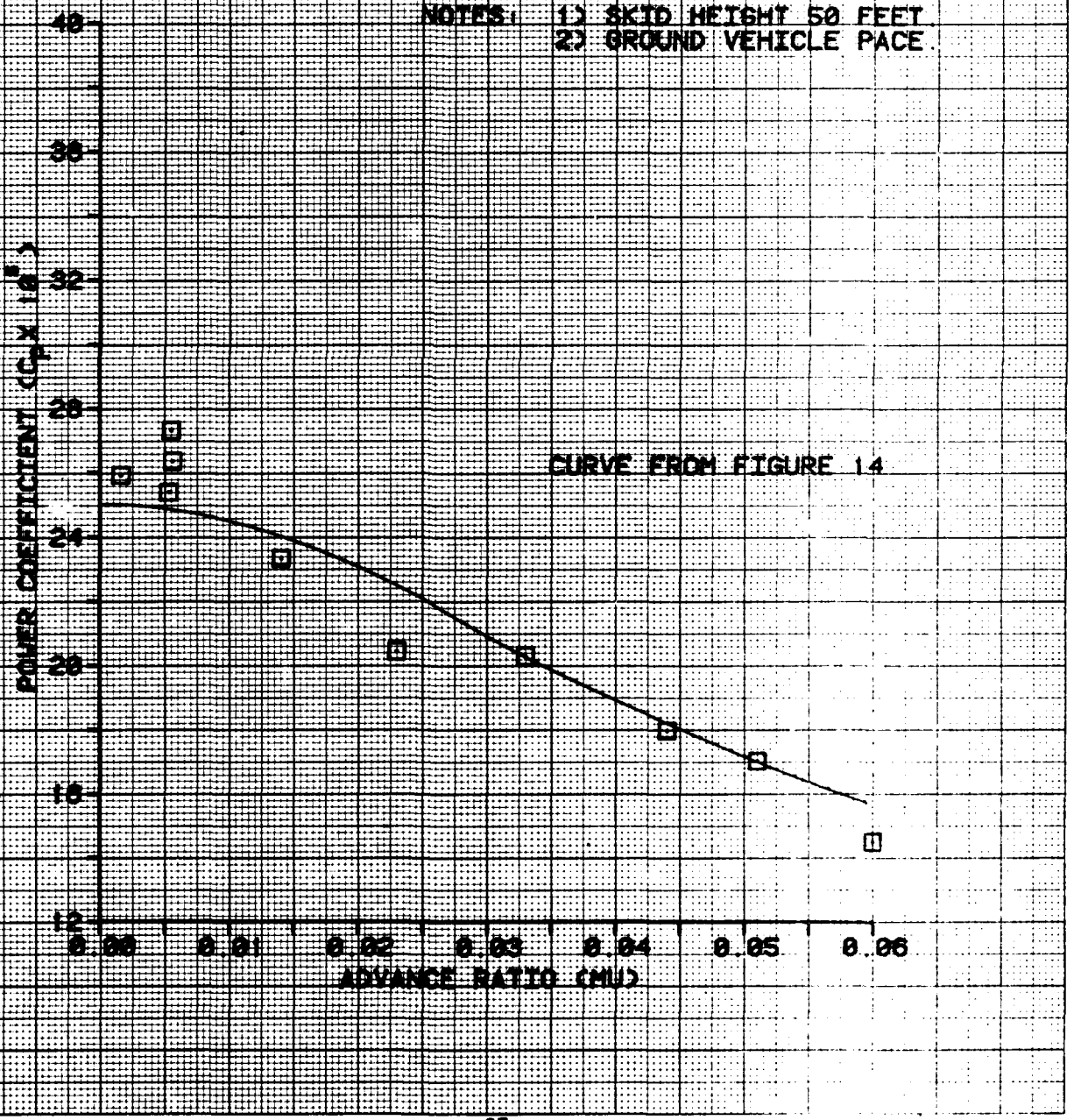

FIGURE 11

NON-DIMENSIONAL LOW-SPEED PERFORMANCE

UH-1H USA S/N 69-15532

SYMBOL	AVG ROTOR SPEED (RPM)	AVG DENSITY ALTITUDE (FEET)	AVG OAT (DEG C)	AVG THRUST COEFFICIENT ($C_T \times 10^4$)
⊡	311	2640	16.0	34.5

NOTES: 1) SKID HEIGHT 50 FEET.
2) GROUND VEHICLE PACE.

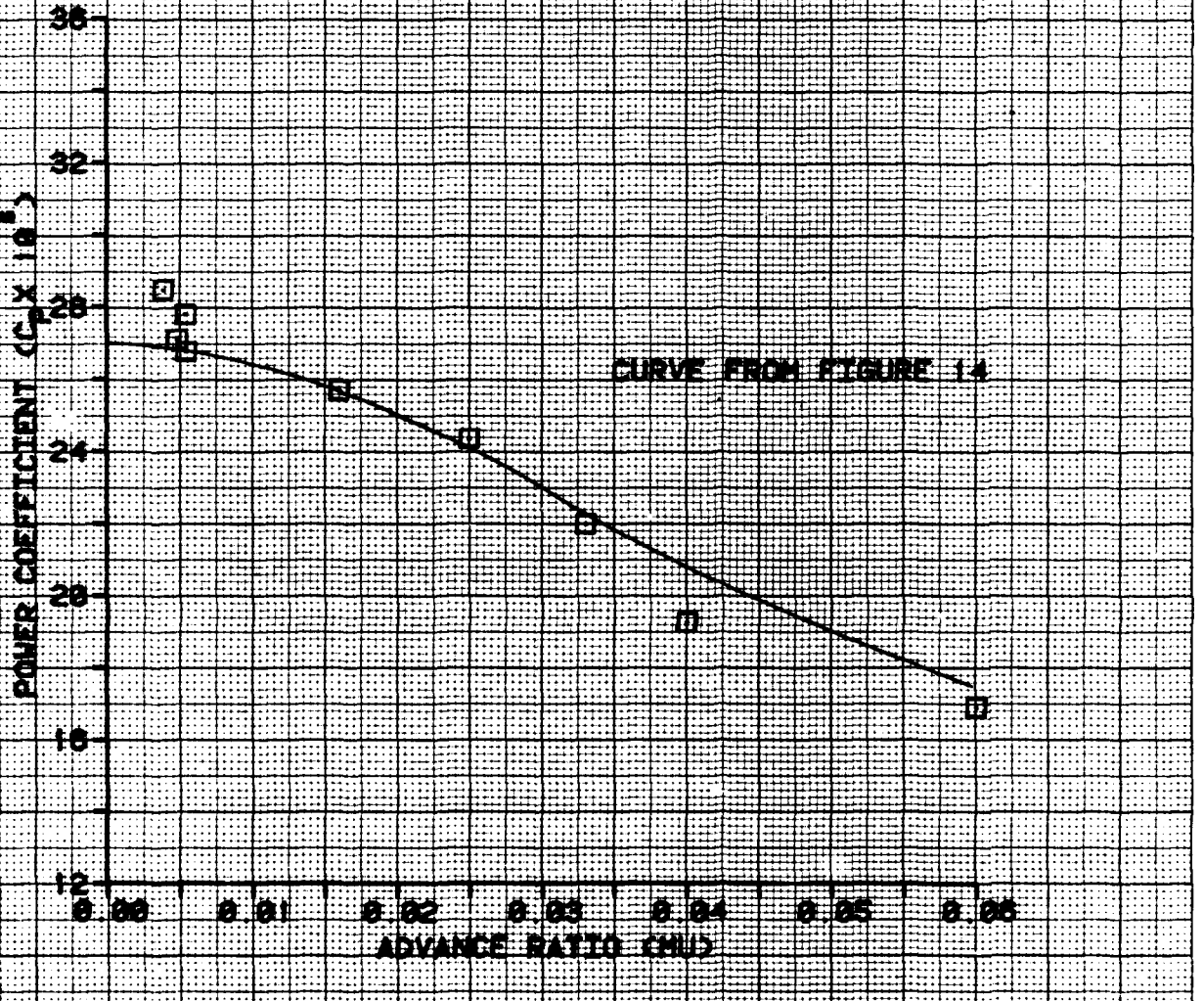

FIGURE 12

NON-DIMENSIONAL LOW-SPEED PERFORMANCE

UH-1H USA S/N 69-15532

SYMBOL	AVG ROTOR SPEED (RPH)	AVG DENSITY ALTITUDE (FEET)	AVG OAT (DEG C)	AVG THRUST COEFFICIENT ($C_T \times 10^4$)
⊡	321	2000	14.0	35.4

NOTES: 1) SKID HEIGHT 50 FEET.
2) GROUND VEHICLE PACE.

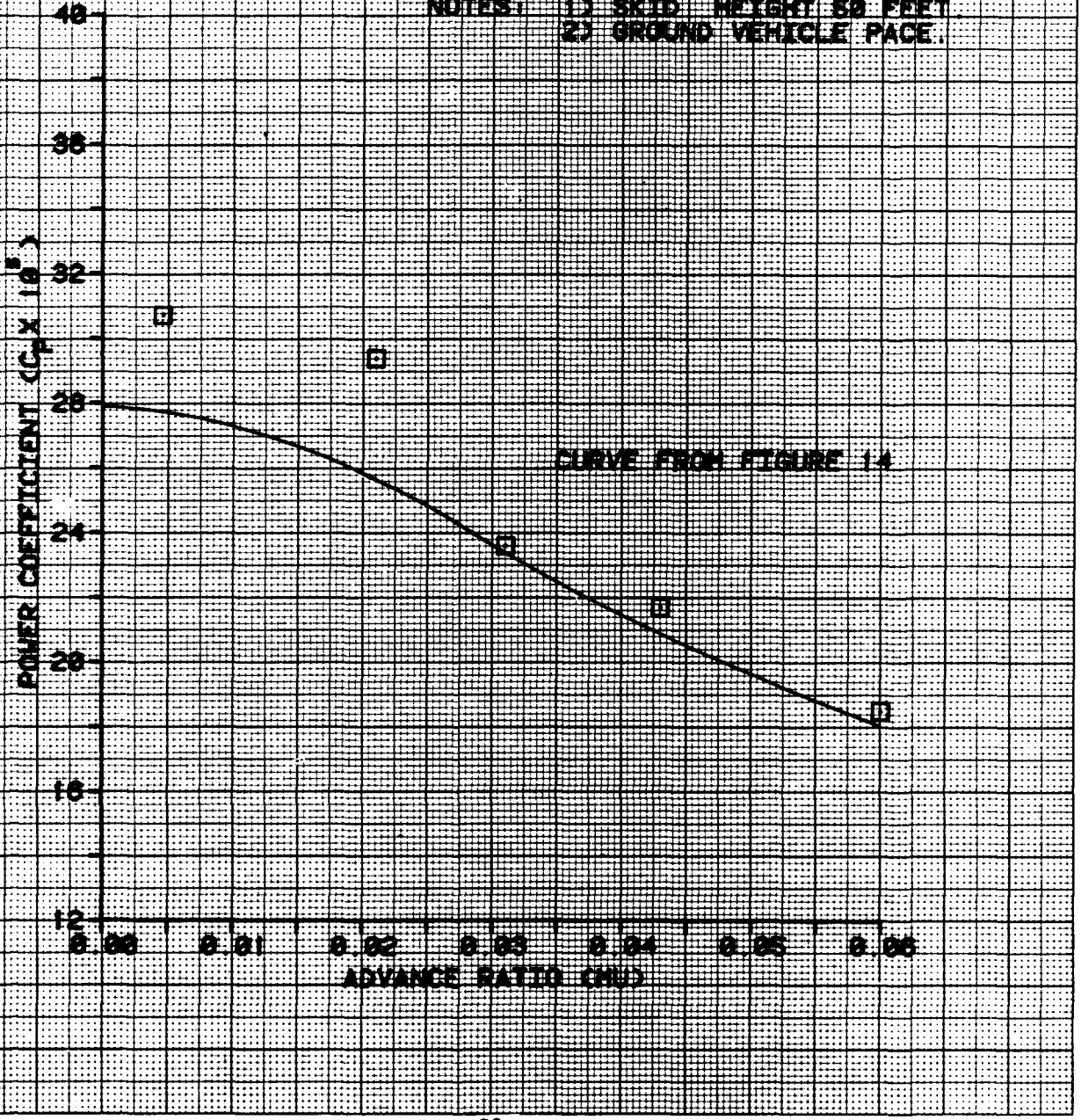

FIGURE 13

NON-DIMENSIONAL LOW-SPEED PERFORMANCE

UH-1H USA S/N 66-15532

SYMBOL	AVG ROTOR SPEED (RPM)	AVG DENSITY ALTITUDE (FEET)	AVG OAT (DEG C)	AVG THRUST COEFFICIENT ($C_T X 10^4$)
□	311	2700	14.4	37.0

NOTES: 1) SKID HEIGHT 50 FEET.
2) GROUND VEHICLE PACE.

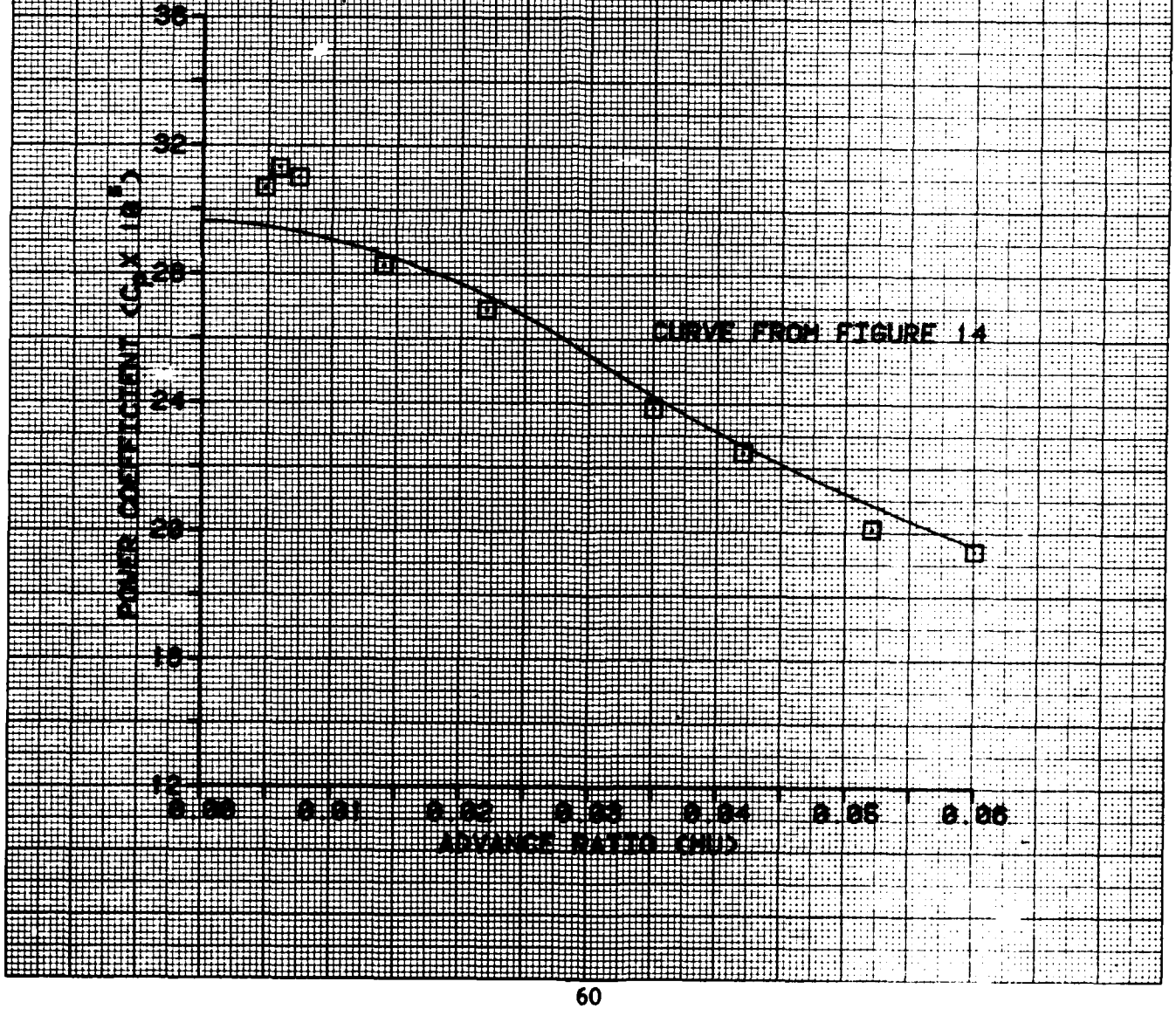

FIGURE 14
LOW-SPEED PERFORMANCE SUMMARY
UH-1H USA S/N 66-15532

NOTES: 1) CURVES OBTAINED FROM FIGURES 8 THRU 13.
2) SKID HEIGHT 50 FEET.

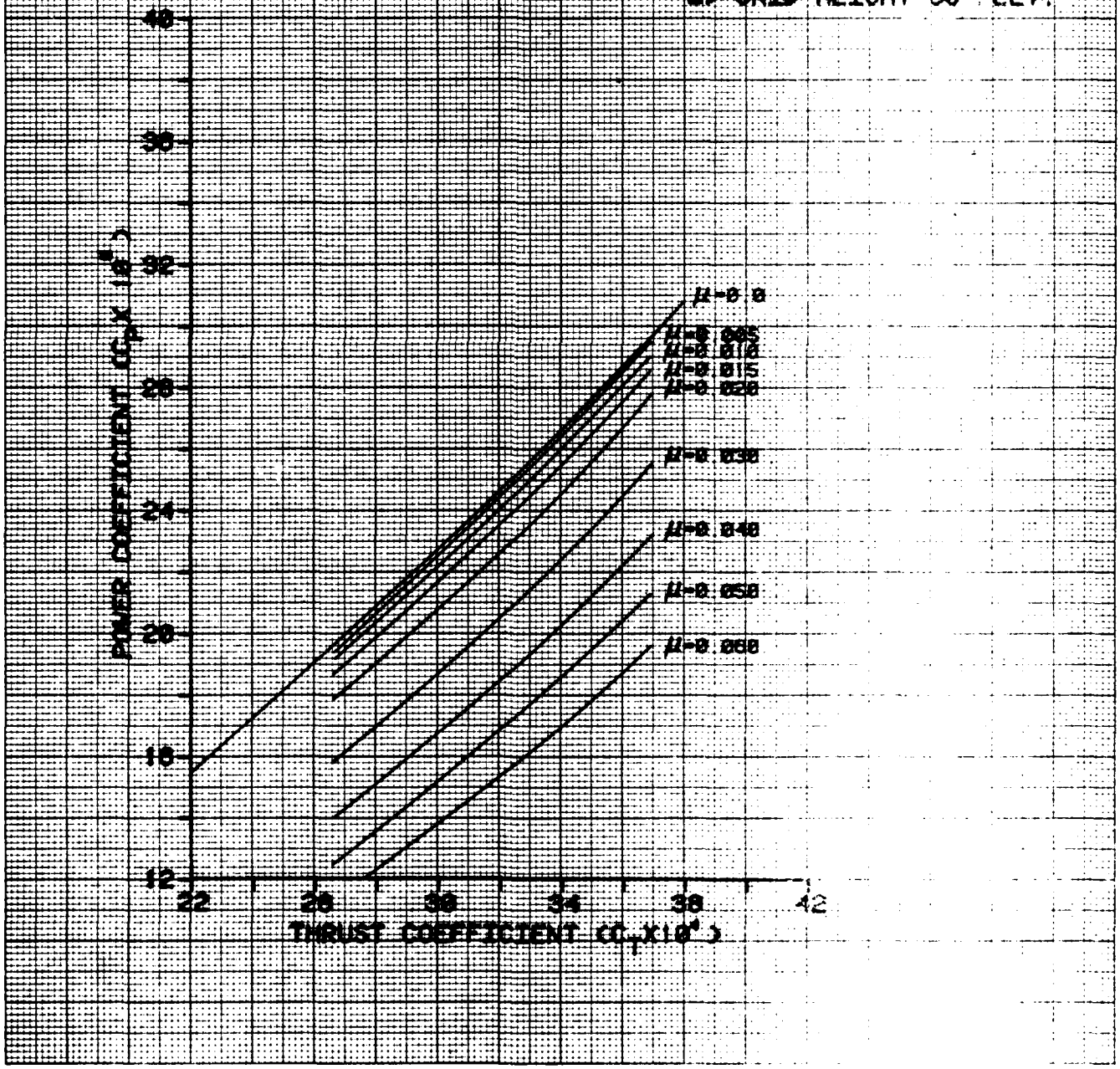

DISTRIBUTION

Deputy Chief of Staff for Logistics (DALO-SMM, DALO-AV)	2
Deputy Chief of Staff Operations (DAMO-RO)	1
Deputy Chief of Staff for Personnel (DAPE-HRS)	1
Deputy Chief of Staff for Research Development and Acquisition (DAMA-PPM-T, DAMA-RA, DAMA-WSA)	3
Comptroller of the Army (DACA-EA)	1
US Army Materiel Development and Readiness Command (DRCDE-SA, DRCQA-E, DRCDE-I, DRCDE-P, DRCQA-SA, DRCSM-WA)	6
US Army Training and Doctrine Command (ATTG-U, ATCD-T, ATCD-ET, ATCD-B)	4
US Army Aviation Systems Command (DRSAV-ED, DRSAV-EI, DRSAV-EL, DRSAV-EA, DRSAV-EP, DRSAV-ES, DRSAV-O, DRSAV-MC, DRSAV-ME)	16
US Army Test and Evaluation Command (DRSTE-CT-A, DRSTE-TO-O)	2
US Army Logistics Evaluation Agency (DALO-LEI)	1
US Army Materiel Systems Analysis Agency (DRXSY-R, DRXSY-MP)	2
US Army Operational Test and Evaluation Agency (CSTE-POD)	1
US Army Armor Center (ATZK-CD-TE)	1
US Army Aviation Center (ATZQ-D-T, ATZQ-TSM-A, ATZQ-TSM-S, ATZQ-TSM-U)	4
US Army Combined Arms Center (ATZLCA-DM)	1
US Army Safety Center (IGAR-TA, IGAR-Library)	2

US Army Research and Technology Laboratories (AVSCOM) (DAVDL-AS, DAVDL-POM (Library))	2
US Army Research and Technology Laboratories/Applied Technology Laboratory (SAVDL-ATL-D, SAVDL-Library)	2
US Army Research and Technology Laboratories/Aeromechanics Laboratory (AVSCOM) (SAVDL-AL-D)	2
US Army Research and Technology Laboratories/Proplusion Laboratory (AVSCOM) (SAVDL-PL-D)	1
Defense Technical Information Center (DDR)	12
US Military Academy (MADN-F)	1
MTMC-TEA (MTT-TRC)	1
ASD/AFXT	1
Director, NASA, Ames Research Center (FHI 237-3 (64/LAH))	3
NASA HO (John Ward, Don Marden, Dick Tobiason, Roger Windblade)	4
Federal Aviation Administration, Technical Center (ANA-70)	3
NASA/Lewis Research Center (MS 86-7)	3